9. Quantum Chromodynamics

Revised September 2017 by S. Bethke (Max-Planck-Institute of Physics, Munich), G. Dissertori (ETH Zurich), and G.P. Salam (CERN).[1]

This update retains the 2016 summary of α_s values, as few new results were available at the deadline for this Review. Those and further new results will be included in the next update.

9.1. Basics

Quantum Chromodynamics (QCD), the gauge field theory that describes the strong interactions of colored quarks and gluons, is the SU(3) component of the SU(3)×SU(2)×U(1) Standard Model of Particle Physics.

The Lagrangian of QCD is given by

$$\mathcal{L} = \sum_q \bar{\psi}_{q,a}(i\gamma^\mu \partial_\mu \delta_{ab} - g_s \gamma^\mu t^C_{ab} \mathcal{A}^C_\mu - m_q \delta_{ab})\psi_{q,b} - \frac{1}{4} F^A_{\mu\nu} F^{A\,\mu\nu} \,, \tag{9.1}$$

where repeated indices are summed over. The γ^μ are the Dirac γ-matrices. The $\psi_{q,a}$ are quark-field spinors for a quark of flavor q and mass m_q, with a color-index a that runs from $a = 1$ to $N_c = 3$, *i.e.* quarks come in three "colors." Quarks are said to be in the fundamental representation of the SU(3) color group.

The $\mathcal{A}^C_\mu$ correspond to the gluon fields, with C running from 1 to $N_c^2 - 1 = 8$, *i.e.* there are eight kinds of gluon. Gluons transform under the adjoint representation of the SU(3) color group. The t^C_{ab} correspond to eight 3×3 matrices and are the generators of the SU(3) group (*cf.* the section on "SU(3) isoscalar factors and representation matrices" in this *Review*, with $t^C_{ab} \equiv \lambda^C_{ab}/2$). They encode the fact that a gluon's interaction with a quark rotates the quark's color in SU(3) space. The quantity g_s is the QCD coupling constant. Finally, the field tensor $F^A_{\mu\nu}$ is given by

$$F^A_{\mu\nu} = \partial_\mu \mathcal{A}^A_\nu - \partial_\nu \mathcal{A}^A_\mu - g_s\, f_{ABC} \mathcal{A}^B_\mu \mathcal{A}^C_\nu \qquad [t^A, t^B] = i f_{ABC} t^C \,, \tag{9.2}$$

where the f_{ABC} are the structure constants of the SU(3) group.

Neither quarks nor gluons are observed as free particles. Hadrons are color-singlet (*i.e.* color-neutral) combinations of quarks, anti-quarks, and gluons.

Ab-initio predictive methods for QCD include lattice gauge theory and perturbative expansions in the coupling. The Feynman rules of QCD involve a quark-antiquark-gluon ($q\bar{q}g$) vertex, a 3-gluon vertex (both proportional to g_s), and a 4-gluon vertex (proportional to g_s^2). A full set of Feynman rules is to be found for example in Ref. 1.

Useful color-algebra relations include: $t^A_{ab} t^A_{bc} = C_F \delta_{ac}$, where $C_F \equiv (N_c^2 - 1)/(2N_c) = 4/3$ is the color-factor ("Casimir") associated with gluon emission from a quark;

[1] On leave from LPTHE, UMR 7589, CNRS, Paris, France

$f_{ACD}f_{BCD} = C_A\delta_{AB}$ where $C_A \equiv N_c = 3$ is the color-factor associated with gluon emission from a gluon; $t^A_{ab}t^B_{ab} = T_R\delta_{AB}$, where $T_R = 1/2$ is the color-factor for a gluon to split to a $q\bar{q}$ pair.

The fundamental parameters of QCD are the coupling g_s (or $\alpha_s = \frac{g_s^2}{4\pi}$) and the quark masses m_q.

There is freedom for an additional CP-violating term to be present in the QCD Lagrangian, $\theta\frac{\alpha_s}{8\pi}F^A_{\mu\nu}\tilde{F}^{A\,\mu\nu}$, where $\tilde{F}^{A\,\mu\nu}$ is the dual of the gluon field tensor, $\frac{1}{2}\epsilon_{\mu\nu\sigma\rho}F^{A\,\sigma\rho}$, where $\epsilon_{\mu\nu\sigma\rho}$ is the fully antisymmetric Levi-Cevita symbol. Experimental limits on the neutron electric dipole moment [2] constrain the coefficient of this contribution to satisfy $|\theta| \lesssim 10^{-10}$. Further discussion is to be found in Ref. 3 and in the Axions section in the Listings of this *Review*.

This section will concentrate mainly on perturbative aspects of QCD as they relate to collider physics. Related textbooks and reviews include Refs. 1,4–8. Aspects specific to Monte Carlo event generators are reviewed in the dedicated section 41. Lattice QCD is also reviewed in a section of its own, Sec. 17, with further discussion of perturbative and non-perturbative aspects to be found in the sections on "Quark Masses", "The CKM quark-mixing matrix", "Structure Functions", "Fragmentation Functions", and "Heavy-Quark and Soft-Collinear Effective Theory" in this *Review*. For an overview of some of the QCD issues and recent results in heavy-ion physics, see for example Refs. [9–11].

9.1.1. *Running coupling* :

In the framework of perturbative QCD (pQCD), predictions for observables are expressed in terms of the renormalized coupling $\alpha_s(\mu_R^2)$, a function of an (unphysical) renormalization scale μ_R. When one takes μ_R close to the scale of the momentum transfer Q in a given process, then $\alpha_s(\mu_R^2 \simeq Q^2)$ is indicative of the effective strength of the strong interaction in that process.

The coupling satisfies the following renormalization group equation (RGE):

$$\mu_R^2\frac{d\alpha_s}{d\mu_R^2} = \beta(\alpha_s) = -(b_0\alpha_s^2 + b_1\alpha_s^3 + b_2\alpha_s^4 + \cdots) \tag{9.3}$$

where $b_0 = (11C_A - 4n_fT_R)/(12\pi) = (33 - 2n_f)/(12\pi)$ is referred to as the 1-loop β-function coefficient, the 2-loop coefficient is $b_1 = (17C_A^2 - n_fT_R(10C_A + 6C_F))/(24\pi^2) = (153 - 19n_f)/(24\pi^2)$, and the 3-loop coefficient is $b_2 = (2857 - \frac{5033}{9}n_f + \frac{325}{27}n_f^2)/(128\pi^3)$ for the SU(3) values of C_A and C_F. The 4-loop coefficient, b_3, is to be found in Refs. 12, 13, while the 5-loop coefficient, b_4, is in Refs. 14–16. The coefficients b_2 and b_3 (and beyond) are renormalization-scheme-dependent, and given here in the modified minimal subtraction ($\overline{\rm MS}$) scheme [17], by far the most widely used scheme in QCD.

The minus sign in Eq. (9.3) is the origin of Asymptotic Freedom [18,19], *i.e.* the fact that the strong coupling becomes weak for processes involving large momentum transfers ("hard processes"). For momentum transfers in the 100 GeV – TeV range, $\alpha_s \sim 0.1$, while the theory is strongly interacting for scales around and below 1 GeV.

The β-function coefficients, the b_i, are given for the coupling of an *effective theory* in which n_f of the quark flavors are considered light ($m_q \ll \mu_R$), and in which the remaining heavier quark flavors decouple from the theory. One may relate the coupling for the theory with $n_f + 1$ light flavors to that with n_f flavors through an equation of the form

$$\alpha_s^{(n_f+1)}(\mu_R^2) = \alpha_s^{(n_f)}(\mu_R^2) \left(1 + \sum_{n=1}^{\infty} \sum_{\ell=0}^{n} c_{n\ell} \, [\alpha_s^{(n_f)}(\mu_R^2)]^n \ln^\ell \frac{\mu_R^2}{m_h^2} \right) , \tag{9.4}$$

where m_h is the mass of the $(n_f+1)^{\text{th}}$ flavor, and the first few $c_{n\ell}$ coefficients are $c_{11} = \frac{1}{6\pi}$, $c_{10} = 0$, $c_{22} = c_{11}^2$, $c_{21} = \frac{19}{24\pi^2}$, and $c_{20} = -\frac{11}{72\pi^2}$ when m_h is the $\overline{\text{MS}}$ mass at scale m_h ($c_{20} = \frac{7}{24\pi^2}$ when m_h is the pole mass — mass definitions are discussed below and in the review on "Quark Masses"). Terms up to $c_{4\ell}$ are to be found in Refs. 20, 21. Numerically, when one chooses $\mu_R = m_h$, the matching is a modest effect, owing to the zero value for the c_{10} coefficient. Relations between n_f and (n_f+2) flavors where the two heavy flavors are close in mass are given to three loops in Ref. 22.

Working in an energy range where the number of flavors is taken constant, a simple exact analytic solution exists for Eq. (9.3) only if one neglects all but the b_0 term, giving $\alpha_s(\mu_R^2) = (b_0 \ln(\mu_R^2/\Lambda^2))^{-1}$. Here Λ is a constant of integration, which corresponds to the scale where the perturbatively-defined coupling would diverge. Its value is indicative of the energy range where non-perturbative dynamics dominates. A convenient approximate analytic solution to the RGE that includes the terms up to b_4 is given by the iterative solution of Eq. (9.3)

$$\begin{aligned}
\alpha_s(\mu_R^2) \simeq \frac{1}{b_0 t} \Bigg(1 - \frac{b_1}{b_0^2} \frac{\ell}{t} + \frac{b_1^2(\ell^2 - \ell - 1) + b_0 b_2}{b_0^4 t^2} + \\
+ \frac{b_1^3 \left(-2\ell^3 + 5\ell^2 + 4\ell - 1\right) - 6 b_0 b_2 b_1 \ell + b_0^2 b_3}{2 b_0^6 t^3} + \\
+ \frac{18 b_0 b_2 b_1^2 \left(2\ell^2 - \ell - 1\right) + b_1^4 \left(6\ell^4 - 26\ell^3 - 9\ell^2 + 24\ell + 7\right)}{6 b_0^8 t^4} \\
+ \frac{-b_0^2 b_3 b_1 (12\ell + 1) + 2 b_0^2 \left(5 b_2^2 + b_0 b_4\right)}{6 b_0^8 t^4} \Bigg),
\end{aligned} \tag{9.5}$$

with $t \equiv \ln \frac{\mu_R^2}{\Lambda^2}$ and $\ell = \ln t$, again parametrized in terms of a constant Λ. Note that Eq. (9.5) is one of several possible approximate 4-loop solutions for $\alpha_s(\mu_R^2)$, and that a value for Λ only defines $\alpha_s(\mu_R^2)$ once one knows which particular approximation is being used. An alternative to the use of formulas such as Eq. (9.5) is to solve the RGE exactly, numerically (including the discontinuities, Eq. (9.4), at flavor thresholds). In such cases the quantity Λ does directly arise (though it can be defined, cf. Eqs. (1–3) of Ref.24). For these reasons, in determinations of the coupling, it has become standard practice to

quote the value of α_s at a given scale (typically the mass of the Z boson, M_Z) rather than to quote a value for Λ.

The value of the coupling, as well as the exact forms of the b_2, c_{10} (and higher-order) coefficients, depend on the renormalization scheme in which the coupling is defined, *i.e.* the convention used to subtract infinities in the context of renormalization. The coefficients given above hold for a coupling defined in the $\overline{\rm MS}$ scheme.

A discussion of determinations of the coupling and a graph illustrating its scale dependence ("running") are to be found in Section 9.4. The RunDec package [25,26,27] is often used to calculate the evolution of the coupling. For a discussion of electroweak effects in the evolution of the QCD coupling, see Ref. 28 and references therein.

9.1.2. *Quark masses* :

Free quarks have never been observed, which is understood as a result of a long-distance, confining property of the strong QCD force: up, down, strange, charm, and bottom quarks all *hadronize*, *i.e.* become part of a meson or baryon, on a timescale $\sim 1/\Lambda$; the top quark instead decays before it has time to hadronize. This means that the question of what one means by the quark mass is a complex one, which requires that one adopts a specific prescription. A perturbatively defined prescription is the pole mass, m_q, which corresponds to the position of the divergence of the propagator. This is close to one's physical picture of mass. However, when relating it to observable quantities, it suffers from substantial non-perturbative ambiguities (see *e.g.* Ref. 29). An alternative is the $\overline{\rm MS}$ mass, $\overline{m}_q(\mu_R^2)$, which depends on the renormalization scale μ_R.

Results for the masses of heavier quarks are often quoted either as the pole mass or as the $\overline{\rm MS}$ mass evaluated at a scale equal to the mass, $\overline{m}_q(\overline{m}_q^2)$; light quark masses are often quoted in the $\overline{\rm MS}$ scheme at a scale $\mu_R \sim 2$ GeV. The pole and $\overline{\rm MS}$ masses are related by a slowly converging series that starts $m_q = \overline{m}_q(\overline{m}_q^2)(1 + \dfrac{4\alpha_s(\overline{m}_q^2)}{3\pi} + \mathcal{O}(\alpha_s^2))$, while the scale-dependence of $\overline{\rm MS}$ masses is given by

$$\mu_R^2 \frac{d\overline{m}_q(\mu_R^2)}{d\mu_R^2} = \left[-\frac{\alpha_s(\mu_R^2)}{\pi} + \mathcal{O}(\alpha_s^2) \right] \overline{m}_q(\mu_R^2)\,. \tag{9.6}$$

More detailed discussion is to be found in a dedicated section of the *Review*, "Quark Masses.", with detailed formulas also in Ref. 30 and references therein.

In perturbative QCD calculations of scattering processes, it is common to work in an approximation in which one neglects (*i.e.* sets to zero) the masses of all quarks whose mass is significantly smaller than the momentum transfer in the process.

9.2. Structure of QCD predictions

9.2.1. *Fully inclusive cross sections* :

The simplest observables in perturbative QCD are those that do not involve initial-state hadrons and that are fully inclusive with respect to details of the final state. One example is the total cross section for $e^+e^- \to$ hadrons at center-of-mass energy Q, for which one can write

$$\frac{\sigma(e^+e^- \to \text{hadrons}, Q)}{\sigma(e^+e^- \to \mu^+\mu^-, Q)} \equiv R(Q) = R_{\text{EW}}(Q)(1 + \delta_{\text{QCD}}(Q))\,, \tag{9.7}$$

where $R_{\text{EW}}(Q)$ is the purely electroweak prediction for the ratio and $\delta_{\text{QCD}}(Q)$ is the correction due to QCD effects. To keep the discussion simple, we can restrict our attention to energies $Q \ll M_Z$, where the process is dominated by photon exchange ($R_{\text{EW}} = 3\sum_q e_q^2$, neglecting finite-quark-mass corrections, where the e_q are the electric charges of the quarks),

$$\delta_{\text{QCD}}(Q) = \sum_{n=1}^{\infty} c_n \cdot \left(\frac{\alpha_s(Q^2)}{\pi}\right)^n + \mathcal{O}\left(\frac{\Lambda^4}{Q^4}\right)\,. \tag{9.8}$$

The first four terms in the α_s series expansion are then to be found in Ref. 31,

$$c_1 = 1\,, \qquad c_2 = 1.9857 - 0.1152 n_f\,, \tag{9.9a}$$

$$c_3 = -6.63694 - 1.20013 n_f - 0.00518 n_f^2 - 1.240\eta\,, \tag{9.9b}$$

$$c_4 = -156.61 + 18.775 n_f - 0.7974 n_f^2 + 0.0215 n_f^3 - (17.828 - 0.575 n_f)\eta\,, \tag{9.9c}$$

with $\eta = (\sum e_q)^2/(3\sum e_q^2)$. For corresponding expressions including also Z exchange and finite-quark-mass effects, see Refs. [32–34].

A related series holds also for the QCD corrections to the hadronic decay width of the τ lepton, which essentially involves an integral of $R(Q)$ over the allowed range of invariant masses of the hadronic part of the τ decay (see *e.g.* Ref. 35). The series expansions for QCD corrections to Higgs-boson hadronic (partial) decay widths are summarized in Refs. 36, 37, 38.

One characteristic feature of Eqs. (9.8) and (9.9) is that the coefficients of α_s^n increase order by order: calculations in perturbative QCD tend to converge more slowly than would be expected based just on the size of α_s[††]. Another feature is the existence of an extra "power-correction" term $\mathcal{O}(\Lambda^4/Q^4)$ in Eq. (9.8), which accounts for contributions that are fundamentally non-perturbative. All high-energy QCD predictions involve such corrections, though the exact power of Λ/Q depends on the observable. For many

[††] The situation is significantly worse near thresholds, *e.g.* the $t\bar{t}$ production threshold. An overview of some of the methods used in such cases is to be found for example in Ref. 39.

processes and observables, it is possible to introduce an operator product expansion and associate power suppressed terms with specific higher-dimension (non-perturbative) operators.

Scale dependence. In Eq. (9.8) the renormalization scale for α_s has been chosen equal to Q. The result can also be expressed in terms of the coupling at an arbitrary renormalization scale μ_R,

$$\delta_{\rm QCD}(Q) = \sum_{n=1}^{\infty} \overline{c}_n\left(\frac{\mu_R^2}{Q^2}\right) \cdot \left(\frac{\alpha_s(\mu_R^2)}{\pi}\right)^n + \mathcal{O}\left(\frac{\Lambda^4}{Q^4}\right) , \tag{9.10}$$

where $\overline{c}_1(\mu_R^2/Q^2) \equiv c_1$, $\overline{c}_2(\mu_R^2/Q^2) = c_2 + \pi b_0 c_1 \ln(\mu_R^2/Q^2)$, $\overline{c}_3(\mu_R^2/Q^2) = c_3 + (2b_0c_2\pi + b_1c_1\pi^2)\ln(\mu_R^2/Q^2) + b_0^2c_1\pi^2\ln^2(\mu_R^2/Q^2)$, *etc.* Given an infinite number of terms in the α_s expansion, the μ_R dependence of the $\overline{c}_n(\mu_R^2/Q^2)$ coefficients will exactly cancel that of $\alpha_s(\mu_R^2)$, and the final result will be independent of the choice of μ_R: physical observables do not depend on unphysical scales.**

With just terms up to some finite $n = N$, a residual μ_R dependence will remain, which implies an uncertainty on the prediction of $R(Q)$ due to the arbitrariness of the scale choice. This uncertainty will be $\mathcal{O}(\alpha_s^{N+1})$, *i.e.* of the same order as the neglected terms. For this reason it is customary to use QCD predictions' scale dependence as an estimate of the uncertainties due to neglected terms. One usually takes a central value for $\mu_R \sim Q$, in order to avoid the poor convergence of the perturbative series that results from the large $\ln^{n-1}(\mu_R^2/Q^2)$ terms in the $\overline{c}_n$ coefficients when $\mu_R \ll Q$ or $\mu_R \gg Q$. Uncertainties are then commonly determined by varying μ_R by a factor of two up and down around the central scale choice, as discussed in more detail below in Section 9.2.4.

9.2.2. *Processes with initial-state hadrons* :

Deep Inelastic Scattering. To illustrate the key features of QCD cross sections in processes with initial-state hadrons, let us consider deep-inelastic scattering (DIS), $ep \to e + X$, where an electron e with four-momentum k emits a highly off-shell photon (momentum q) that interacts with the proton (momentum p). For photon virtualities $Q^2 \equiv -q^2$ far above the squared proton mass (but far below the Z mass), the differential cross section in terms of the kinematic variables Q^2, $x = Q^2/(2p\cdot q)$ and $y = (q\cdot p)/(k\cdot p)$ is

$$\frac{d^2\sigma}{dxdQ^2} = \frac{4\pi\alpha^2}{2xQ^4}\left[(1+(1-y)^2)F_2(x,Q^2) - y^2F_L(x,Q^2)\right] , \tag{9.11}$$

** There is an important caveat to this statement: at sufficiently high orders, perturbative series generally suffer from "renormalon" divergences $\alpha_s^n n!$ (reviewed in Ref. 29). This phenomenon is not usually visible with the limited number of perturbative terms available today. However it is closely connected with non-perturbative contributions and sets a limit on the possible precision of perturbative predictions. The cancellation of scale dependence will also ultimately be affected by this renormalon-induced breakdown of perturbation theory.

where α is the electromagnetic coupling and $F_2(x,Q^2)$ and $F_L(x,Q^2)$ are proton structure functions, which encode the interaction between the photon (in given polarization states) and the proton. In the presence of parity-violating interactions (*e.g.* νp scattering) an additional F_3 structure function is present. For an extended review, including equations for the full electroweak and polarized cases, see Sec. 18 of this *Review*.

Structure functions are not calculable in perturbative QCD, nor is any other cross section that involves initial-state hadrons. To zeroth order in α_s, the structure functions are given directly in terms of non-perturbative parton (quark or gluon) distribution functions (PDFs),

$$F_2(x,Q^2) = x\sum_q e_q^2 f_{q/p}(x)\,, \qquad F_L(x,Q^2) = 0\,, \tag{9.12}$$

where $f_{q/p}(x)$ is the PDF for quarks of type q inside the proton, *i.e.* the number density of quarks of type q inside a fast-moving proton that carry a fraction x of its longitudinal momentum (the quark flavor index q, here, is not to be confused with the photon momentum q in the lines preceding Eq. (9.11)). PDFs are non-perturbative, and only just starting to be extracted in lattice QCD in a phenomenologically relevant way [40] and there is also some debate about the underlying methods [41]. Accordingly, for all practical uses, they are determined from data (*cf.* Sec. 18 of this *Review* and also Ref. 42).

The above result, with PDFs $f_{q/p}(x)$ that are independent of the scale Q, corresponds to the "quark-parton model" picture in which the photon interacts with point-like free quarks, or equivalently, one has incoherent elastic scattering between the electron and individual constituents of the proton. As a consequence, in this picture also F_2 and F_L are independent of Q [43]. When including higher orders in pQCD, Eq. (9.12) becomes

$$\begin{aligned} F_2(x,Q^2) = x\sum_{n=0}^{\infty}\frac{\alpha_s^n(\mu_R^2)}{(2\pi)^n}\sum_{i=q,g}\int_x^1\frac{dz}{z}C_{2,i}^{(n)}(z,Q^2,\mu_R^2,\mu_F^2)\,f_{i/p}\Big(\frac{x}{z},\mu_F^2\Big) \\ + \mathcal{O}\Big(\frac{\Lambda^2}{Q^2}\Big)\,. \end{aligned} \tag{9.13}$$

Just as in Eq. (9.10), we have a series in powers of $\alpha_s(\mu_R^2)$, each term involving a coefficient $C_{2,i}^{(n)}$ that can be calculated using Feynman graphs. An important difference is the additional integral over z. The parton that comes from the proton can emit a gluon before it interacts with the photon. As a result, the $C_{2,i}^{(n)}$ coefficients are functions that depend on the ratio, z, of the parton's momentum before and after the gluon emission, and one must integrate over that ratio. For the electromagnetic component of DIS with light quarks and gluons, the zeroth order coefficient functions are $C_{2,q}^{(0)} = e_q^2\delta(1-z)$ and $C_{2,g}^{(0)} = 0$. Corrections are known up to $\mathcal{O}(\alpha_s^3)$ (next-to-next-next-to-leading order, N^{3}LO) for both electromagnetic [44] and weak currents [45,46]. For heavy-quark production they are known to $\mathcal{O}(\alpha_s^2)$ [47] (next-to-leading order, NLO, insofar as the series starts at $\mathcal{O}(\alpha_s)$), with ongoing work towards NNLO summarized in Ref. 48.

The majority of the emissions that modify a parton's momentum are collinear (parallel) to that parton, and don't depend on the fact that the parton is destined to interact with a photon. It is natural to view these emissions as modifying the proton's structure rather than being part of the coefficient function for the parton's interaction with the photon. Technically, one uses a procedure known as *collinear factorization* to give a well-defined meaning to this distinction, most commonly through the $\overline{\rm MS}$ factorization scheme, defined in the context of dimensional regularization. The $\overline{\rm MS}$ factorization scheme involves an arbitrary choice of *factorization scale*, μ_F, whose meaning can be understood roughly as follows: emissions with transverse momenta above μ_F are included in the $C^{(n)}_{2,q}(z, Q^2, \mu_R^2, \mu_F^2)$; emissions with transverse momenta below μ_F are accounted for within the PDFs, $f_{i/p}(x, \mu_F^2)$. While collinear factorization is generally believed to be valid for suitable (sufficiently inclusive) observables in processes with hard scales, Ref. 49, which reviews the factorization proofs in detail, is cautious in the statements it makes about their exhaustivity, notably for the hadron-collider processes that we shall discuss below. Further discussion is to be found in Refs. 50,51.

The PDFs' resulting dependence on μ_F is described by the Dokshitzer-Gribov-Lipatov-Altarelli-Parisi (DGLAP) equations [52], which to leading order (LO) read*

$$\mu_F^2 \frac{\partial f_{i/p}(x,\mu_F^2)}{\partial \mu_F^2} = \sum_j \frac{\alpha_s(\mu_F^2)}{2\pi} \int_x^1 \frac{dz}{z} P^{(1)}_{i\leftarrow j}(z) f_{j/p}\left(\frac{x}{z}, \mu_F^2\right), \tag{9.14}$$

with, for example, $P^{(1)}_{q\leftarrow g}(z) = T_R(z^2 + (1-z)^2)$. The other LO splitting functions are listed in Sec. 18 of this *Review*, while results up to NLO, α_s^2, and NNLO, α_s^3, are given in Refs. 53 and 54 respectively. A significant part ("non-singlet") of the N^{3}LO results is given in Ref. 55. Splitting functions for polarized PDFs are given in Ref. 56. Beyond LO, the coefficient functions are also μ_F dependent, for example $C^{(1)}_{2,i}(x, Q^2, \mu_R^2, \mu_F^2) = C^{(1)}_{2,i}(x, Q^2, \mu_R^2, Q^2) - \ln\left(\frac{\mu_F^2}{Q^2}\right) \sum_j \int_x^1 \frac{dz}{z} C^{(0)}_{2,j}(\frac{x}{z}) P^{(1)}_{j\leftarrow i}(z)$. In certain contexts, higher-order QED and mixed QED-QCD corrections to the splitting functions are also needed [57].

As with the renormalization scale, the choice of factorization scale is arbitrary, but if one has an infinite number of terms in the perturbative series, the μ_F-dependences of the coefficient functions and PDFs will compensate each other fully. Given only N terms of the series, a residual $\mathcal{O}(\alpha_s^{N+1})$ uncertainty is associated with the ambiguity in

* LO is generally taken to mean the lowest order at which a quantity is non-zero. This definition is nearly always unambiguous, the one major exception being for the case of the hadronic branching ratio of virtual photons, Z, τ, *etc.*, for which two conventions exist: LO can either mean the lowest order that contributes to the hadronic branching fraction, *i.e.* the term "1" in Eq. (9.7); or it can mean the lowest order at which the hadronic branching ratio becomes sensitive to the coupling, $n = 1$ in Eq. (9.8), as is relevant when extracting the value of the coupling from a measurement of the branching ratio. Because of this ambiguity, we avoid use of the term "LO" in that context.

the choice of μ_F. As with μ_R, varying μ_F provides an input in estimating uncertainties on predictions. In inclusive DIS predictions, the default choice for the scales is usually $\mu_R = \mu_F = Q$.

As is the case for the running coupling, in DGLAP evolution one can introduce flavor thresholds near the heavy quark masses: below a given heavy quark's mass, that quark is not considered to be part of the proton's structure, while above it is considered to be part of the proton's structure and evolves with massless DGLAP splitting kernels. With appropriate parton distribution matching terms at threshold, such a variable flavor number scheme (VFNS), when used with massless coefficient functions, gives the full heavy-quark contributions at high Q^2 scales. For scales near the threshold, it is instead necessary to appropriately adapt the standard massive coefficient functions to account for the heavy-quark contribution already included in the PDFs [58,59,60].

Hadron-hadron collisions. The extension to processes with two initial-state hadrons can be illustrated with the example of the total (inclusive) cross section for W boson production in collisions of hadrons h_1 and h_2, which can be written as

$$\sigma(h_1 h_2 \to W + X) = \sum_{n=0}^{\infty} \alpha_s^n(\mu_R^2) \sum_{i,j} \int dx_1 dx_2 \, f_{i/h_1}\left(x_1, \mu_F^2\right) f_{j/h_2}\left(x_2, \mu_F^2\right) \times \hat{\sigma}^{(n)}_{ij\to W+X}\left(x_1 x_2 s, \mu_R^2, \mu_F^2\right) + \mathcal{O}\left(\frac{\Lambda^2}{M_W^4}\right) , \tag{9.15}$$

where s is the squared center-of-mass energy of the collision. At LO, $n = 0$, the hard (partonic) cross section $\hat{\sigma}^{(0)}_{ij\to W+X}(x_1 x_2 s, \mu_R^2, \mu_F^2)$ is simply proportional to $\delta(x_1 x_2 s - M_W^2)$, in the narrow W-boson width approximation (see Sec. 49 of this *Review* for detailed expressions for this and other hard scattering cross sections). It is non-zero only for choices of i, j that can directly give a W, such as $i = u$, $j = \bar{d}$. At higher orders, $n \geq 1$, new partonic channels contribute, such as gq, and there is no restriction $x_1 x_2 s = M_W^2$.

Equation (9.15) involves a collinear factorization between the hard cross section and the PDFs, just like Eq. (9.13). As long as the same factorization scheme is used in DIS and pp or $p\bar{p}$ (usually the $\overline{\text{MS}}$ scheme), then PDFs extracted in DIS can be directly used in pp and $p\bar{p}$ predictions [61,49] (with the anti-quark distributions in an anti-proton being the same as the quark distributions in a proton).

Fully inclusive hard cross sections are known to NNLO, *i.e.* corrections up to relative order α_s^2, for Drell-Yan (DY) lepton-pair and vector-boson production [62,63], Higgs-boson production in association with a vector boson [64], Higgs-boson production via vector-boson fusion [65] (in an approximation that factorizes the production of the two vector bosons), Higgs-pair production [66], top-antitop production [67] and vector-boson pair production [68,69]. † Recently, inclusive Higgs production through gluon fusion and

† Processes with jets or photons in the final state have divergent cross sections unless one places cut on the jet or photon momentum. Accordingly they are discussed below in Section 9.2.3.2.

vector-boson fusion were calculated at N^{3}LO [70,71]. A discussion of many other Higgs results is to be found in Ref. 72.

Photoproduction. γp (and $\gamma\gamma$) collisions are similar to pp collisions, with the subtlety that the photon can behave in two ways: there is "direct" photoproduction, in which the photon behaves as a point-like particle and takes part directly in the hard collision, with hard subprocesses such as $\gamma g \to q\bar{q}$; there is also resolved photoproduction, in which the photon behaves like a hadron, with non-perturbative partonic substructure and a corresponding PDF for its quark and gluon content, $f_{i/\gamma}(x, Q^2)$.

While useful to understand the general structure of γp collisions, the distinction between direct and resolved photoproduction is not well defined beyond leading order, as discussed for example in Ref. 73.

The high-energy (BFKL) limit. In situations in which the total center-of-mass energy $\sqrt{s}$ is much larger than all other momentum-transfer scales in the problem (*e.g.* Q in DIS, m_b for $b\bar{b}$ production in pp collisions, *etc.*), each power of α_s beyond LO can be accompanied by a power of $\ln(s/Q^2)$ (or $\ln(s/m_b^2)$, *etc.*). This is variously referred to as the high-energy, small-x or Balitsky-Fadin-Kuraev-Lipatov (BFKL) limit [74–76]. Currently it is possible to account for the dominant and first subdominant [77,78] power of $\ln s$ at each order of α_s, and also to estimate further subdominant contributions that are numerically large (see Refs. 79–82 and references therein). Progress towards NNLO is discussed in Ref. 83.

Physically, the summation of all orders in α_s can be understood as leading to a growth with s of the gluon density in the proton. At sufficiently high energies this implies non-linear effects (commonly referred to as parton saturation), whose treatment has been the subject of intense study (see for example Refs. 84, 85 and references thereto). Note that it is not straightforward to relate these results to the genuinely non-perturbative total, elastic and diffractive cross sections for hadron-hadron scattering (experimental results for which are summarized in section 51 of this *Review*).

9.2.3. *Non fully inclusive cross sections* :

QCD final states always consist of hadrons, while perturbative QCD calculations deal with partons. Physically, an energetic parton fragments ("showers") into many further partons, which then, on later timescales, undergo a transition to hadrons ("hadronization"). Fixed-order perturbation theory captures only a small part of these dynamics.

This does not matter for the fully inclusive cross sections discussed above: the showering and hadronization stages are approximately unitary, *i.e.* they do not substantially change the overall probability of hard scattering, because they occur long after it has taken place (they introduce at most a correction proportional to a power of the ratio of timescales involved, *i.e.* a power of Λ/Q, where Q is the hard scattering scale).

Less inclusive measurements, in contrast, may be affected by the extra dynamics. For those sensitive just to the main directions of energy flow (jet rates, event shapes, *cf.* Sec. 9.3.1) fixed order perturbation theory is often still adequate, because showering and hadronization don't substantially change the overall energy flow. This means that one

can make a prediction using just a small number of partons, which should correspond well to a measurement of the same observable carried out on hadrons. For observables that instead depend on distributions of individual hadrons (which, *e.g.*, are the inputs to detector simulations), it is mandatory to account for showering and hadronization. The range of predictive techniques available for QCD final states reflects this diversity of needs of different measurements.

While illustrating the different methods, we shall for simplicity mainly use expressions that hold for e^+e^- scattering. The extension to cases with initial-state partons will be mostly straightforward (space constraints unfortunately prevent us from addressing diffraction and exclusive hadron-production processes; extensive discussion is to be found in Refs. 86, 87).

9.2.3.1. *Soft and collinear limits:*

Before examining specific predictive methods, it is useful to be aware of a general property of QCD matrix elements in the soft and collinear limits. Consider a squared tree-level matrix element $|M_n^2(p_1,\ldots,p_n)|$ for the process $e^+e^- \to n$ partons with momenta $p_1,\ldots,p_n$, and a corresponding phase-space integration measure $d\Phi_n$. If particle n is a gluon, and additionally it becomes collinear (parallel) to another particle i and its momentum tends to zero (it becomes "soft"), the matrix element simplifies as follows,

$$\lim_{\theta_{in}\to 0,\, E_n\to 0} d\Phi_n |M_n^2(p_1,\ldots,p_n)| \\ = d\Phi_{n-1}|M_{n-1}^2(p_1,\ldots,p_{n-1})| \frac{\alpha_s C_i}{\pi}\frac{d\theta_{in}^2}{\theta_{in}^2}\frac{dE_n}{E_n}\,, \tag{9.16}$$

where $C_i = C_F$ (C_A) if i is a quark (gluon). This formula has non-integrable divergences both for the inter-parton angle $\theta_{in} \to 0$ and for the gluon energy $E_n \to 0$, which are mirrored also in the structure of divergences in loop diagrams. These divergences are important for at least two reasons: firstly, they govern the typical structure of events (inducing many emissions either with low energy or at small angle with respect to hard partons); secondly, they will determine which observables can be calculated within perturbative QCD.

9.2.3.2. *Fixed-order predictions:*

Let us consider an observable $\mathcal{O}$ that is a function $\mathcal{O}_n(p_1,\ldots,p_n)$ of the four-momenta of the n final-state particles in an event (whether partons or hadrons). In what follows, we shall consider the cross section for events weighted with the value of the observable, $\sigma_{\mathcal{O}}$. As examples, if $\mathcal{O}_n \equiv 1$ for all n, then $\sigma_{\mathcal{O}}$ is just the total cross section; if $\mathcal{O}_n \equiv \hat{\tau}(p_1,\ldots,p_n)$ where $\hat{\tau}$ is the value of the Thrust for that event (see Sec. 9.3.1.2), then the average value of the Thrust is $\langle\tau\rangle = \sigma_{\mathcal{O}}/\sigma_{\rm tot}$; if $\mathcal{O}_n \equiv \delta(\tau - \hat{\tau}(p_1,\ldots,p_n))$ then one gets the differential cross section as a function of the Thrust, $\sigma_{\mathcal{O}} \equiv d\sigma/d\tau$.

In the expressions below, we shall omit to write the non-perturbative power correction term, which for most common observables is proportional to a single power of Λ/Q.

LO. If the observable $\mathcal{O}$ is non-zero only for events with at least n final-state particles, then the LO QCD prediction for the weighted cross section in e^+e^- annihilation is

$$\sigma_{\mathcal{O},LO} = \alpha_s^{n-2}(\mu_R^2) \int d\Phi_n |M_n^2(p_1,\ldots,p_n)|\, \mathcal{O}_n(p_1,\ldots,p_n)\,, \tag{9.17}$$

where the squared tree-level matrix element, $|M_n^2(p_1,\ldots,p_n)|$, includes relevant symmetry factors, has been summed over all subprocesses (*e.g.* $e^+e^- \to q\bar{q}q\bar{q}$, $e^+e^- \to q\bar{q}gg$) and has had all factors of α_s extracted in front. In processes other than e^+e^- collisions, the center-of-mass energy of the LO process is generally not fixed, and so the powers of the coupling are often brought inside the integrals, with the scale μ_R chosen event by event, as a function of the event kinematics.

Other than in the simplest cases (see the review on Cross Sections in this *Review*), the matrix elements in Eq. (9.17) are usually calculated automatically with programs such as CompHEP [88], MadGraph [89], Alpgen [90], Comix/Sherpa [91], and Helac/Phegas [92]. Some of these (CompHEP, MadGraph) use formulas obtained from direct evaluations of Feynman diagrams. Others (Alpgen, Helac/Phegas and Comix/Sherpa) use methods designed to be particularly efficient at high multiplicities, such as Berends-Giele recursion [93], which builds up amplitudes for complex processes from simpler ones (see also the reviews and discussion in Refs. [94–96]).

The phase-space integration is usually carried out by Monte Carlo sampling, in order to deal with the sometimes complicated cuts that are used in corresponding experimental measurements. Because of the divergences in the matrix element, Eq. (9.16), the integral converges only if the observable vanishes for kinematic configurations in which one of the n particles is arbitrarily soft or it is collinear to another particle. As an example, the cross section for producing any configuration of n partons will lead to an infinite integral, whereas a finite result will be obtained for the cross section for producing n deposits of energy (or jets, see Sec. 9.3.1.1), each above some energy threshold and well separated from each other in angle.

LO calculations can be carried out for $2 \to n$ processes with $n \lesssim 6-10$. The exact upper limit depends on the process, the method used to evaluate the matrix elements (recursive methods are more efficient), and the extent to which the phase-space integration can be optimized to work around the large variations in the values of the matrix elements.

NLO. Given an observable that is non-zero starting from n final-state particles, its prediction at NLO involves supplementing the LO result, Eq. (9.17), with the $2 \to (n+1)$-particle squared tree-level matrix element ($|M_{n+1}^2|$), and the interference of an $2 \to n$ tree-level and $2 \to n$ 1-loop amplitude ($2\mathrm{Re}(M_n M^*_{n,1-\mathrm{loop}})$),

$$\begin{aligned}\sigma_{\mathcal{O}}^{NLO} = \sigma_{\mathcal{O}}^{LO} &+ \alpha_s^{n-1}(\mu_R^2) \int d\Phi_{n+1} |M_{n+1}^2(p_1,\ldots,p_{n+1})|\, \mathcal{O}_{n+1}(p_1,\ldots,p_{n+1}) \\ &+ \alpha_s^{n-1}(\mu_R^2) \int d\Phi_n\, 2\mathrm{Re}\,[\, M_n(p_1,\ldots,p_n) \\ &\qquad M^*_{n,1-\mathrm{loop}}(p_1,\ldots,p_n)\,]\, \mathcal{O}_n(p_1,\ldots,p_n)\,. \end{aligned} \tag{9.18}$$

Relative to LO calculations, two important issues appear in the NLO calculations. Firstly, the extra complexity of loop-calculations relative to tree-level calculations means that their automation has been achieved only in recent years (see below). Secondly, loop amplitudes are infinite in 4 dimensions, while tree-level amplitudes are finite, but their *integrals* are infinite, due to the divergences of Eq. (9.16). These two sources of infinities have the same soft and collinear origins and cancel after the integration only if the observable $\mathcal{O}$ satisfies the property of infrared and collinear safety,

$$\begin{aligned} &\mathcal{O}_{n+1}(p_1,\ldots,p_s,\ldots,p_n) &&\to \mathcal{O}_n(p_1,\ldots,p_n) && \text{if } p_s \to 0 \\ &\mathcal{O}_{n+1}(p_1,\ldots,p_a,p_b,\ldots,p_n) &&\to \mathcal{O}_n(p_1,\ldots,p_a+p_b,\ldots,p_n) \\ & && \text{if } p_a \,||\, p_b\,. \end{aligned} \tag{9.19}$$

Examples of infrared-safe quantities include event-shape distributions and jet cross sections (with appropriate jet algorithms, see below). Unsafe quantities include the distribution of the momentum of the hardest QCD particle (which is not conserved under collinear splitting), observables that require the complete absence of radiation in some region of phase space (*e.g.* rapidity gaps or 100% isolation cuts, which are affected by soft emissions), or the particle multiplicity (affected by both soft and collinear emissions). The non-cancellation of divergences at NLO due to infrared or collinear unsafety compromises the usefulness not only of the NLO calculation, but also that of a LO calculation, since LO is only an acceptable approximation if one can prove that higher-order terms are smaller. Infrared and collinear unsafety usually also imply large non-perturbative effects.

As with LO calculations, the phase-space integrals in Eq. (9.18) are usually carried out by Monte Carlo integration, so as to facilitate the study of arbitrary observables. Various methods exist to obtain numerically efficient cancellation among the different infinities. These include notably dipole [97], FKS [98] and antenna [99] subtraction.

NLO calculations exist for a wide range of processes. Historically, many calculations have been performed process by process and are available in dedicated packages, among them NLOJet++ [100] for e^+e^-, DIS, and hadron-hadron processes involving just light partons in the final state, MCFM [101] for hadron-hadron processes with Higgs or vector bosons and/or heavy quarks in the final state, VBFNLO for vector-boson fusion, di- and tri-boson processes [102], and the Phox family [103] for processes with photons in the final state. Many of these programs are still widely used today.

Recent years have seen very active development of automated NLO calculational tools, and a number of programs are available publicly: Madgraph5_aMC@NLO [89] and Helac-NLO [104] provide full frameworks for NLO calculations; GoSam [105], Njet [106], OpenLoops [107] and Recola [108] calculate just the 1-loop part and are typically interfaced with an external tool such as Sherpa [109] for combination with the appropriate tree-level amplitudes. Another tool, BlackHat [110] is available publicly in a pre-release form, and many of its results can be accessed in the form of ntuples [111] to which a range of cuts, and histogramming options, as well as PDF and scale-changes, can be applied *a posteriori*; an alternative approach for *a posteriori* PDF and scale change represents NLO (or NNLO) results, for a given set of cuts and binning, as an effective coefficient function on a grid in parton momentum fractions and factorization scales [112–115].

In some cases the above programs (or development versions of them) can be used to calculate also NLO electroweak or beyond-standard-model corrections [116–119]. Electroweak corrections are especially important for transverse momenta significantly above the W and Z masses, because they are enhanced by two powers of $\ln p_t/M_W$ for each power of the electroweak coupling.

The above tools rely in part on a wide array of developments reviewed in Refs. 95,120. Examples of the most complex processes for which NLO QCD corrections have been obtained so far include $e^+e^- \to 7$ jets [121], $pp \to W + 5$ jets [122] and $pp \to 5$ jets [123].

NNLO. Conceptually, NNLO and NLO calculations are similar, except that one must add a further order in α_s, consisting of: the squared $(n+2)$-parton tree-level amplitude, the interference of the $(n+1)$-parton tree-level and 1-loop amplitudes, the interference of the n-parton tree-level and 2-loop amplitudes, and the squared n-parton 1-loop amplitude.

Each of these elements involves large numbers of soft and collinear divergences, satisfying relations analogous to Eq. (9.16) that now involve multiple collinear or soft particles and higher loop orders (see *e.g.* Refs. [124–126]). Arranging for the cancellation of the divergences after numerical Monte Carlo integration has been one of the significant challenges of NNLO calculations, as has the determination of the relevant 2-loop amplitudes. For the cancellations of divergences a wide range of methods has been developed. Some of them [127–131] retain the approach, inherent in NLO methods, of directly combining the separate loop and tree-level amplitudes. Others combine a suitably chosen, partially inclusive $2 \to n$ NNLO calculation with a fully differential $2 \to n+1$ NLO calculation [132–135].

Quite a number of processes have been calculated differentially at NNLO so far. The state of the art for e^+e^- collisions is $e^+e^- \to 3$ jets [136–138]. For Deep Inelastic Scattering, dijet production is known at NNLO [139]. For hadron colliders, all $2 \to 1$ processes are known, specifically vector boson [140,141] and Higgs boson production [142,132]. For most of the above calculations there exist public codes (EERAD3 for e^+e^-, DYNNLO and FEWZ for W and Z production, fehipro and HNNLO for Higgs production), links to which are to be found among the above references. Substantial progress has been made in the past couple of years for hadron-collider $2 \to 2$ processes, with calculations having been performed for nearly all relevant processes: HH [66] (in large-top-mass approximation, see also the exact (two-loop) NLO result [143]) , WH [144] and ZH [145], ZZ [69] WW [68] and WZ [146], $\gamma\gamma$ [147,148], $Z\gamma$ [149] and $W\gamma$ [150] (many of these colour singlet processes are available also in MCFM [151]), $H+$jet [152,153,154,155], $W+$jet [133], $Z+$jet [156,157] and $\gamma+$jet [158], t-channel single-top [159,160], $t\bar{t}$ production [161], and dijet production [162]. One $2 \to 3$ process is known at NNLO, Higgs production through vector-boson fusion, using an approximation in which the two underlying DIS-like $q \to qV$ scatterings are factorised [135].

9.2.3.3. *Resummation:*

Many experimental measurements place tight constraints on emissions in the final state. For example, in e^+e^- events, that (one minus) the Thrust should be less than some value $\tau \ll 1$, or in $pp \to Z$ events that the Z-boson transverse momentum should be much smaller than its mass, $p_t^Z \ll M_Z$. A further example is the production of heavy particles or jets near threshold (so that little energy is left over for real emissions) in DIS and pp collisions.

In such cases, the constraint vetoes a significant part of the integral over the soft and collinear divergence of Eq. (9.16). As a result, there is only a partial cancellation between real emission terms (subject to the constraint) and loop (virtual) contributions (not subject to the constraint), causing each order of α_s to be accompanied by a large coefficient $\sim L^2$, where *e.g.* $L = \ln \tau$ or $L = \ln(M_Z/p_t^Z)$. One ends up with a perturbative series whose terms go as $\sim (\alpha_s L^2)^n$. It is not uncommon that $\alpha_s L^2 \gg 1$, so that the perturbative series converges very poorly if at all.** In such cases one may carry out a "resummation," which accounts for the dominant logarithmically enhanced terms to all orders in α_s, by making use of known properties of matrix elements for multiple soft and collinear emissions, and of the all-orders properties of the divergent parts of virtual corrections, following original works such as Refs. 163–172 and also through soft-collinear effective theory [173,174] (*cf.* also the section on "Heavy-Quark and Soft-Collinear Effective Theory" in this *Review*, as well as Ref. 175).

For cases with double logarithmic enhancements (two powers of logarithm per power of α_s), there are two classification schemes for resummation accuracy. Writing the cross section including the constraint as $\sigma(L)$ and the unconstrained (total) cross section as $\sigma_{\rm tot}$, the series expansion takes the form

$$\sigma(L) \simeq \sigma_{\rm tot} \sum_{n=0}^{\infty} \sum_{k=0}^{2n} R_{nk} \alpha_s^n(\mu_R^2) L^k, \qquad L \gg 1 \tag{9.20}$$

and leading log (LL) resummation means that one accounts for all terms with $k = 2n$, next-to-leading-log (NLL) includes additionally all terms with $k = 2n-1$, *etc.* Often $\sigma(L)$ (or its Fourier or Mellin transform) *exponentiates* ‡,

$$\sigma(L) \simeq \sigma_{\rm tot} \exp\left[\sum_{n=1}^{\infty} \sum_{k=0}^{n+1} G_{nk} \alpha_s^n(\mu_R^2) L^k\right], \qquad L \gg 1\,, \tag{9.21}$$

** To be precise one should be aware of two causes of the divergence of perturbative series. That which interests us here is associated with the presence of a new large parameter (*e.g.* ratio of scales). It is distinct from the "renormalon" induced factorial divergences of perturbation theory that were discussed above.

‡ Whether or not this happens depends on the quantity being resummed. A classic example involves jet rates in e^+e^- collisions as a function of a jet-resolution parameter $y_{\rm cut}$. The logarithms of $1/y_{\rm cut}$ exponentiate for the k_t (Durham) jet algorithm [176], but not [177] for the JADE algorithm [178] (both are discussed below in Sec. 9.3.1.1).

where one notes the different upper limit on k ($\leq n+1$) compared to Eq. (9.20). This is a more powerful form of resummation: the G_{12} term alone reproduces the full LL series in Eq. (9.20). With the form Eq. (9.21) one still uses the nomenclature LL, but this now means that all terms with $k = n+1$ are included, and NLL implies all terms with $k = n$, *etc.*

For a large number of observables, NLL resummations are available in the sense of Eq. (9.21) (see Refs. 179–181 and references therein). NNLL has been achieved for the DY and Higgs-boson p_t distributions [182–185] (also available in the CuTe [186], HRes [187] and ResBos [188] families of programs and also differentially in vector-boson decay products [189]) and related variables [190], for the p_t of vector-boson pairs [191], for the back-to-back energy-energy correlation in e^+e^- [192], the jet broadening in e^+e^- collisions [193], the jet-veto survival probability in Higgs and Z boson production in pp collisions [194], an event-shape type observable known as the beam Thrust [195], hadron-collider jet masses in specific limits [196] (see also Ref. 197), the production of top anti-top pairs near threshold [198–200] (and references therein), and high-p_t W and Z production [201]. Automation of NNLL jet-veto resummations for different processes has been achieved in Ref. 202 (*cf.* also the NLL automation in Ref. 203), while automation for a certain class of e^+e^- observables has been achieved in Ref. 204. N^{3}LL resummations are available for the Thrust variable, C-parameter and heavy-jet mass in e^+e^- annihilations [205–207] (confirmed for Thrust at NNLL in Ref. 208), for the Higgs p_t distribution [209] and for for Higgs- and vector-boson production near threshold [210]. An extensive discussion of jet masses for heavy-quark induced jets has been given in Ref. 211 (see also Ref. 212). Recently, there has also been progress in resummed calculations for jet substructure, whose observables involve more complicated definitions than is the case for standard resummations [213–217]. The inputs and methods involved in these various calculations are somewhat too diverse to discuss in detail here, so we recommend that the interested reader consult the original references for further details.

9.2.3.4. *Fragmentation functions:*

Since the parton-hadron transition is non-perturbative, it is not possible to perturbatively calculate quantities such as the energy-spectra of specific hadrons in high-energy collisions. However, one can factorize perturbative and non-perturbative contributions via the concept of fragmentation functions. These are the final-state analogue of the parton distribution functions that are used for initial-state hadrons. Like parton distribution functions, they depend on a (fragmentation) factorization scale and satisfy a DGLAP evolution equation.

It should be added that if one ignores the non-perturbative difficulties and just calculates the energy and angular spectrum of partons in perturbative QCD with some low cutoff scale $\sim \Lambda$ (using resummation to sum large logarithms of $\sqrt{s}/\Lambda$), then this reproduces many features of the corresponding hadron spectra [218]. This is often taken to suggest that hadronization is "local", in the sense it mainly involves partons that are close both in position and in momentum.

Section 19 of this *Review* provides further information (and references) on these topics, including also the question of heavy-quark fragmentation.

9.2.3.5. *Parton-shower Monte Carlo generators:*

Parton-shower Monte Carlo (MC) event generators like PYTHIA [219–221], HERWIG [222–224] and SHERPA [109] provide fully exclusive simulations of QCD events.† Because they provide access to "hadron-level" events, they are a crucial tool for all applications that involve simulating the response of detectors to QCD events. Here we give only a brief outline of how they work and refer the reader to Sec. 41 and Ref. 226 for a full overview.

The MC generation of an event involves several stages. It starts with the random generation of the kinematics and partonic channels of whatever *hard scattering process* the user has requested at some high scale Q_0 (for complex processes, this may be carried out by an external program). This is followed by a *parton shower*, usually based on the successive random generation of gluon emissions (or $g \to q\bar{q}$ splittings). Each is generated at a scale lower than the previous emission, following a (soft and collinear resummed) perturbative QCD distribution that depends on the momenta of all previous emissions. Common choices of scale for the ordering of emissions are virtuality, transverse momentum or angle. Parton showering stops at a scale of order 1 GeV, at which point a *hadronization model* is used to convert the resulting partons into hadrons. One widely-used model involves stretching a color "string" across quarks and gluons, and breaking it up into hadrons [227,228]. Another breaks each gluon into a $q\bar{q}$ pair and then groups quarks and anti-quarks into colorless "clusters", which then give the hadrons [222]. For pp and γp processes, modeling is also needed to treat the collision between the two hadron remnants, which generates an *underlying event* (UE), usually implemented via additional $2 \to 2$ scatterings ("multiple parton interactions") at a scale of a few GeV, following Ref. 229.

A deficiency of the soft and collinear approximations that underlie parton showers is that they may fail to reproduce the full pattern of hard wide-angle emissions, important, for example, in many new physics searches. It is therefore common to use LO multi-parton matrix elements to generate hard high-multiplicity partonic configurations as additional starting points for the showering, supplemented with some prescription (CKKW [230], MLM [231]) for consistently merging samples with different initial multiplicities.

MCs, as described above, generate cross sections for the requested hard process that are correct at LO. A wide variety of processes are available in MC implementations that are correct to NLO, using the MC@NLO [232] or POWHEG [233] prescriptions, notably through the Madgraph5_aMC@NLO [89], POWHEGBox [234] and Sherpa [91,235] programs. Techniques have also been developed recently to combine NLO plus shower accuracy for different multiplicities of final-state jets [236]. Building in part on some of that work, several groups have also obtained NNLO plus shower accuracy for Drell-Yan and Higgs production [237] as well as a handful of other processes.

† The program ARIADNE [225] has also been widely used for simulating e^+e^- and DIS collisions.

9.2.4. ***Accuracy of predictions*** :

Estimating the accuracy of perturbative QCD predictions is not an exact science. It is often said that LO calculations are accurate to within a factor of two. This is based on experience with NLO corrections in the cases where these are available. In processes involving new partonic scattering channels at NLO and/or large ratios of scales (such as jet observables in processes with vector bosons, or the production of high-p_t jets containing B-hadrons), the ratio of the NLO to LO predictions, commonly called the "K-factor", can be substantially larger than 2.

For calculations beyond LO, a conservative approach to estimate the perturbative uncertainty is to take it to be the last known perturbative order; a more widely used method is to estimate it from the change in the prediction when varying the renormalization and factorization scales around a central value Q that is taken close to the physical scale of the process. A conventional range of variation is $Q/2 < \mu_R, \mu_F < 2Q$. This should not be assumed to always estimate the full uncertainty from missing higher orders, but it does indicate the size of one important known source of higher-order ambiguity.[‡‡]

There does not seem to be a broad consensus on whether μ_R and μ_F should be kept identical or varied independently. One common option is to vary them independently with the restriction $\frac{1}{2}\mu_R < \mu_F < 2\mu_R$ [245]. This limits the risk of misleadingly small uncertainties due to fortuitous cancellations between the μ_F and μ_R dependence when both are varied together, while avoiding the appearance of large logarithms of μ_R^2/μ_F^2 when both are varied completely independently.

Calculations that involve resummations usually have an additional source of uncertainty associated with the choice of argument of the logarithms being resummed, *e.g.* $\ln(2\frac{p_t^Z}{M_Z})$ as opposed to $\ln(\frac{1}{2}\frac{p_t^Z}{M_Z})$. In addition to varying renormalization and factorization scales, it is therefore also advisable to vary the argument of the logarithm by a suitable factor in either direction with respect to the "natural" argument.

The accuracy of QCD predictions is limited also by non-perturbative corrections, which typically scale as a power of Λ/Q. For measurements that are directly sensitive to the structure of the hadronic final state, the corrections are usually linear in Λ/Q. The non-perturbative corrections are further enhanced in processes with a significant underlying event (*i.e.* in pp and $p\bar{p}$ collisions) and in cases where the perturbative cross sections fall steeply as a function of p_t or some other kinematic variable, for example in inclusive jet spectra or dijet mass spectra.

Non-perturbative corrections are commonly estimated from the difference between Monte Carlo events at the parton level and after hadronization. An issue to be aware of with this procedure is that "parton level" is not a uniquely defined concept. For example,

[‡‡] A number of prescriptions also exist for setting the scale automatically, *e.g.* Refs. 238–241, eliminating uncertainties from scale variation, though not from the truncation of the perturbative series itself. Recently, there have also been studies of how to estimate uncertainties from missing higher orders that go beyond scale variations [242,243,244].

in an event generator it depends on a (somewhat arbitrary and tunable) internal cutoff scale that separates the parton showering from the hadronization. In contrast no such cutoff scale exists in a NLO or NNLO partonic calculation. For this reason there are widespread reservations as to the appropriateness of deriving hadronization corrections from a Monte Carlo program and then applying them to NLO or NNLO predictions. There exist alternative methods for estimating hadronization corrections, which attempt to analytically deduce non-perturbative effects in one observable based on measurements of other observables (see the reviews [29,246]). While they directly address the problem of different possible definitions of parton level, it should also be said that they are far less flexible than Monte Carlo programs and not always able to provide equally good descriptions of the data.

9.3. Experimental studies of QCD

Since we are not able to directly measure partons (quarks or gluons), but only hadrons and their decay products, a central issue for every experimental study of perturbative QCD is establishing a correspondence between observables obtained at the partonic and the hadronic level. The only theoretically sound correspondence is achieved by means of *infrared and collinear safe* quantities, which allow one to obtain finite predictions at any order of perturbative QCD.

As stated above, the simplest case of infrared- and collinear-safe observables are total cross sections. More generally, when measuring fully inclusive observables, the final state is not analyzed at all regarding its (topological, kinematical) structure or its composition. Basically the relevant information consists in the rate of a process ending up in a partonic or hadronic final state. In e^+e^- annihilation, widely used examples are the ratios of partial widths or branching ratios for the electroweak decay of particles into hadrons or leptons, such as Z or τ decays, (*cf.* Sec. 9.2.1). Such ratios are often favored over absolute cross sections or partial widths because of large cancellations of experimental and theoretical systematic uncertainties. The strong suppression of non-perturbative effects, $\mathcal{O}(\Lambda^4/Q^4)$, is one of the attractive features of such observables, however, at the same time the sensitivity to radiative QCD corrections is small, which for example affects the statistical uncertainty when using them for the determination of the strong coupling constant. In the case of τ decays not only the hadronic branching ratio is of interest, but also moments of the spectral functions of hadronic tau decays, which sample different parts of the decay spectrum and thus provide additional information. Other examples of fully inclusive observables are structure functions (and related sum rules) in DIS. These are extensively discussed in Sec. 18 of this *Review*.

On the other hand, often the structure or composition of the final state are analyzed and cross sections differential in one or more variables characterizing this structure are of interest. Examples are jet rates, jet substructure, event shapes or transverse momentum distributions of jets or vector bosons in hadron collisions. The case of fragmentation functions, *i.e.* the measurement of hadron production as a function of the hadron momentum relative to some hard scattering scale, is discussed in Sec. 19 of this *Review*.

It is worth mentioning that, besides the correspondence between the parton and hadron level, also a correspondence between the hadron level and the actually measured quantities

in the detector has to be established. The simplest examples are corrections for finite experimental acceptance and efficiencies. Whereas acceptance corrections essentially are of theoretical nature, since they involve extrapolations from the measurable (partial) to the full phase space, other corrections such as for efficiency, resolution and response, are of experimental nature. For example, measurements of differential cross sections such as jet rates require corrections in order to relate, *e.g.* the energy deposits in a calorimeter to the jets at the hadron level. Typically detector simulations and/or data-driven methods are used in order to obtain these corrections. Care should be taken here in order to have a clear separation between the parton-to-hadron level and hadron-to-detector level corrections. Finally, for the sake of an easy comparison to the results of other experiments and/or theoretical calculations, it is suggested to provide, whenever possible, measurements corrected for detector effects and/or all necessary information related to the detector response (*e.g.* the detector response matrix).

9.3.1. *Hadronic final-state observables* :

9.3.1.1. *Jets:*

In hard interactions, final-state partons and hadrons appear predominantly in collimated bunches, which are generically called *jets*. To a first approximation, a jet can be thought of as a hard parton that has undergone soft and collinear showering and then hadronization. Jets are used both for testing our understanding and predictions of high-energy QCD processes, and also for identifying the hard partonic structure of decays of massive particles like top quarks.

In order to map observed hadrons onto a set of jets, one uses a *jet definition*. The mapping involves explicit choices: for example when a gluon is radiated from a quark, for what range of kinematics should the gluon be part of the quark jet, or instead form a separate jet? Good jet definitions are infrared and collinear safe, simple to use in theoretical and experimental contexts, applicable to any type of inputs (parton or hadron momenta, charged particle tracks, and/or energy deposits in the detectors) and lead to jets that are not too sensitive to non-perturbative effects.

An extensive treatment of the topic of jet definitions is given in Ref. 247 (for e^+e^- collisions) and Refs. [248–250]. Here we briefly review the two main classes: cone algorithms, extensively used at older hadron colliders, and sequential recombination algorithms, more widespread in e^+e^- and ep colliders and at the LHC.

Very generically, most (iterative) cone algorithms start with some seed particle i, sum the momenta of all particles j within a cone of opening-angle R, typically defined in terms of (pseudo-)rapidity and azimuthal angle. They then take the direction of this sum as a new seed and repeat until the cone is stable, and call the contents of the resulting stable cone a jet if its transverse momentum is above some threshold $p_{t,\mathrm{min}}$. The parameters R and $p_{t,\mathrm{min}}$ should be chosen according to the needs of a given analysis.

There are many variants of cone algorithm, and they differ in the set of seeds they use and the manner in which they ensure a one-to-one mapping of particles to jets, given that two stable cones may share particles ("overlap"). The use of seed particles

is a problem w.r.t. infrared and collinear safety, and seeded algorithms are generally not compatible with higher-order (or sometimes even leading-order) QCD calculations, especially in multi-jet contexts, as well as potentially subject to large non-perturbative corrections and instabilities. Seeded algorithms (JetCLU, MidPoint, and various other experiment-specific iterative cone algorithms) are therefore to be deprecated. A modern alternative is to use a seedless variant, SISCone [251].

Sequential recombination algorithms at hadron colliders (and in DIS) are characterized by a distance $d_{ij} = \min(k_{t,i}^{2p}, k_{t,j}^{2p})\Delta_{ij}^2/R^2$ between all pairs of particles i, j, where Δ_{ij} is their separation in the rapidity-azimuthal plane, $k_{t,i}$ is the transverse momentum w.r.t. the incoming beams, and R is a free parameter. They also involve a "beam" distance $d_{iB} = k_{t,i}^{2p}$. One identifies the smallest of all the d_{ij} and d_{iB}, and if it is a d_{ij}, then i and j are merged into a new pseudo-particle (with some prescription, a recombination scheme, for the definition of the merged four-momentum). If the smallest distance is a d_{iB}, then i is removed from the list of particles and called a jet. As with cone algorithms, one usually considers only jets above some transverse-momentum threshold $p_{t,\min}$. The parameter p determines the kind of algorithm: $p = 1$ corresponds to the (*inclusive-*)k_t algorithm [176,252,253], $p = 0$ defines the *Cambridge-Aachen* algorithm [254,255], while for $p = -1$ we have the *anti-*k_t algorithm [256]. All these variants are infrared and collinear safe to all orders of perturbation theory. Whereas the former two lead to irregularly shaped jet boundaries, the latter results in cone-like boundaries. The *anti-*k_t algorithm has become the de-facto standard for the LHC experiments.

In e^+e^- annihilations the k_t algorithm [176] uses $y_{ij} = 2\,\min(E_i^2, E_j^2)(1-\cos\theta_{ij})/Q^2$ as distance measure and repeatedly merges the pair with smallest y_{ij}, until all y_{ij} distances are above some threshold $y_{\rm cut}$, the jet resolution parameter. The (pseudo)-particles that remain at this point are called the jets. Here it is $y_{\rm cut}$ (rather than R and $p_{t,\min}$) that should be chosen according to the needs of the analysis. As mentioned earlier, the k_t algorithm has the property that logarithms $\ln(1/y_{\rm cut})$ exponentiate in resummation calculations. This is one reason why it is preferred over the earlier JADE algorithm [178], which uses the distance measure $y_{ij} = 2\,E_i\,E_j\,(1-\cos\theta_{ij})/Q^2$. Note that other variants of sequential recombination algorithms for e^+e^- annhilations, using different definitions of the resolution measure y_{ij}, exhibit much larger sensitivities to fragmentation and hadronization effects than the k_t and JADE algorithms [257].

Efficient implementations of the above algorithms are available through the *FastJet* package [258].

9.3.1.2. *Event Shapes:*

Event-shape variables are functions of the four momenta of the particles in the final state and characterize the topology of an event's energy flow. They are sensitive to QCD radiation (and correspondingly to the strong coupling) insofar as gluon emission changes the shape of the energy flow.

The classic example of an event shape is the *Thrust* [259,260] in e^+e^- annihilations, defined as

$$\hat{\tau} = \max_{\vec{n}_\tau} \frac{\sum_i |\vec{p}_i \cdot \vec{n}_\tau|}{\sum_i |\vec{p}_i|} \,, \tag{9.22}$$

where $\vec{p}_i$ are the momenta of the particles or the jets in the final-state and the maximum is obtained for the Thrust axis $\vec{n}_\tau$. In the Born limit of the production of a perfect back-to-back $q\bar{q}$ pair the limit $\hat{\tau} \to 1$ is obtained, whereas a perfectly spherical many-particle configuration leads to $\hat{\tau} \to 1/2$. Further event shapes of similar nature have been extensively measured at LEP and at HERA, and for their definitions and reviews we refer to Refs. 1,4,246,261,262. The energy-energy correlation function [263], namely the energy-weighted angular distribution of produced hadron pairs, and its associated asymmetry are further shape variables that have been studied in detail at e^+e^- colliders. For hadron colliders the appropriate modification consists in only taking the transverse momentum component [264]. More recently, the event shape *N-jettiness* has been proposed [265], that measures the degree to which the hadrons in the final state are aligned along N jet axes or the beam direction. It vanishes in the limit of exactly N infinitely narrow jets.

Phenomenological discussions of event shapes at hadron colliders can be found in Refs. [265–267]. Measurements of hadronic event-shape distributions have been published by CDF [268], ATLAS [269–273] and CMS [274–276].

Event shapes are used for many purposes. These include measuring the strong coupling, tuning the parameters of Monte Carlo programs, investigating analytical models of hadronization and distinguishing QCD events from events that might involve decays of new particles (giving event-shape values closer to the spherical limit).

9.3.1.3. *Jet substructure, quark vs. gluon jets:*

Jet substructure, which can be resolved by finding subjets or by measuring jet shapes, is sensitive to the details of QCD radiation in the shower development inside a jet and has been extensively used to study differences in the properties of quark and gluon induced jets, strongly related to their different color charges. In general there is clear experimental evidence that gluon jets have a softer particle spectrum and are "broader" than (light-) quark jets, when looking at observables such as the jet shape $\Psi(r/R)$. This is the fractional transverse momentum contained within a sub-cone of cone-size r for jets of cone-size R. It is sensitive to the relative fractions of quark and gluon jets in an inclusive jet sample and receives contributions from soft-gluon initial-state radiation and the underlying event. Therefore, it has been widely employed for validation and tuning of Monte Carlo models. Furthermore, this quantity turns out to be sensitive to the modification of the gluon radiation pattern in heavy ion collisions (see *e.g.* Ref. 277).

The most recent jet shape measurements using proton-proton collision data have been presented for inclusive jet samples [278–280] and for top-quark production [281]. Further discussions, references and recent summaries can be found in Refs. 262, 282, 283 and Sec. 4 of Ref. 284.

The use of jet substructure has also been investigated in order to distinguish QCD jets from jets that originate from hadronic decays of boosted massive particles (high-p_t electroweak bosons, top quarks and hypothesized new particles). Recently, a considerable number of experimental studies have been carried out with Tevatron and LHC data, in order to investigate on the performance of the proposed algorithms for resolving jet substructure and to apply them to searches for new physics, as well as to the

reconstruction of boosted top quarks, vector bosons and the Higgs boson. For reviews of this rapidly growing field, see sec. 5.3 of Ref. 248, Ref. 250 and Refs. [284–289].

9.3.2. ***QCD measurements at colliders*** :

There exists a wealth of data on QCD-related measurements in e^+e^-, ep, pp, and $p\bar{p}$ collisions, to which a short overview like this would not be able to do any justice. Extensive reviews of the subject have been published in Refs. 261, 262 for e^+e^- colliders and in Ref. 290 for ep scattering, whereas for hadron colliders comprehensive overviews are given in, *e.g.*, Refs. 249, 283 and Refs. [291–293].

Below we concentrate our discussion on measurements that are most sensitive to hard QCD processes, with focus on jet production.

9.3.2.1. e^+e^- *colliders:* Analyses of jet production in e^+e^- collisions are mostly based on data from the JADE experiment at center-of-mass energies between 14 and 44 GeV, as well as on LEP collider data at the Z resonance and up to 209 GeV. They cover the measurements of (differential or exclusive) jet rates (with multiplicities typically up to 4, 5 or 6 jets), the study of 3-jet events and particle production between the jets as a tool for testing hadronization models, as well as 4-jet production and angular correlations in 4-jet events.

Event-shape distributions from e^+e^- data have been an important input to the tuning of parton shower MC models, typically matched to matrix elements for 3-jet production. In general these models provide good descriptions of the available, highly precise data. Especially for the large LEP data sample at the Z peak, the statistical uncertainties are mostly negligible and the experimental systematic uncertainties are at the percent level or even below. These are usually dominated by the uncertainties related to the MC model dependence of the efficiency and acceptance corrections (often referred to as "detector corrections").

Observables measured in e^+e^- collisions have been used for determinations of the strong coupling constant (*cf.* Section 9.4 below) and for putting constraints on the QCD color factors (*cf.* Sec. 9.1 for their definitions), thus probing the non-abelian nature of QCD. Typically, cross sections can be expressed as functions of these color factors, for example $\sigma = f(\alpha_s C_F, C_A/C_F, n_f T_R/C_F)$. Angular correlations in 4-jet events give sensitivity at leading order. Some sensitivity to these color factors, although only at NLO, is also obtained from event-shape distributions. Scaling violations of fragmentation functions and the different subjet structure in quark and gluon induced jets also give access to these color factors. In order to extract absolute values, *e.g.* for C_F and C_A, certain assumptions have to be made for other parameters, such as T_R, n_f or α_s, since typically only combinations (ratios, products) of all the relevant parameters appear in the perturbative predictions. A compilation of results [262] quotes world average values of $C_A = 2.89 \pm 0.03(\text{stat}) \pm 0.21(\text{syst})$ and $C_F = 1.30 \pm 0.01(\text{stat}) \pm 0.09(\text{syst})$, with a correlation coefficient of 82%. These results are in perfect agreement with the expectations from SU(3) of $C_A = 3$ and $C_F = 4/3$.

9.3.2.2. *DIS and photoproduction:* Multi-jet production in *ep* collisions at HERA, both in the DIS and photoproduction regime, allows for tests of QCD factorization (one initial-state proton and its associated PDF versus the hard scattering which leads to high-p_t jets) and NLO calculations which exist for 2- and 3-jet final states. Sensitivity is also obtained to the product of the coupling constant and the gluon PDF. Experimental uncertainties of the order of 5–10% have been achieved, mostly dominated by the jet energy scale, whereas statistical uncertainties are negligible to a large extent. For comparison to theoretical predictions, at large jet p_t the PDF uncertainty dominates the theoretical uncertainty (typically of order 5–10%, in some regions of phase space up to 20%), therefore jet observables become useful inputs for PDF fits.

In general, the data are well described by NLO matrix-element calculations, combined with DGLAP evolution equations, in particular at large Q^2 and central values of jet pseudo-rapidity. At low values of Q^2 and x, in particular for large jet pseudo-rapidities, certain features of the data have been interpreted as requiring BFKL-type evolution, though the predictions for such schemes are still limited. It is worth noting that there is lack of consensus throughout the community regarding this need of BFKL-evolution at currently probed x, Q^2 values, and an alternative approach [294] that implements the merging of LO matrix-element based event generation with a parton shower (using the SHERPA framework) successfully describes the data in all kinematical regions, including the low Q^2, low x domain. At moderately small x values, it should perhaps not be surprising that the BFKL approach and fixed-order matrix-element merging with parton showers may both provide adequate descriptions of the data, because some part of the multi-parton phase space that they model is common to both approaches.

In the case of photoproduction, a wealth of measurements with low p_t jets were performed in order to constrain the photon PDFs. The uncertainties related to these photon PDFs play a minor role at high jet p_t, which has allowed for precise tests of pQCD calculations.

A few examples of recent measurements can be found in Refs. 295–303 for DIS and in Refs. 304–308 for photoproduction.

9.3.2.3. *Hadron colliders:* The spectrum of observables and the number of measurements performed at hadron colliders is enormous, probing many regions of phase space and covering a huge range of cross sections, as illustrated in Fig. 9.1 for the case of the ATLAS and CMS experiments at the LHC. For the sake of brevity, in the following only certain classes of those measurements will be discussed, that allow addressing particular aspects of the various QCD studies performed. Most of our discussion will focus on recent LHC results, which are available for center-of-mass energies of 2.76, 5, 7, 8 and 13 TeV with integrated luminosities of up to $36\,\mathrm{fb}^{-1}$. Generally speaking, besides representing a general test of the standard model and QCD in particular, these measurements serve several purposes, such as: (i) probing pQCD and its various approximations and implementations in MC models, in order to quantify the order of magnitude of not yet calculated contributions and to gauge their precision when used as background predictions, or (ii) extracting/constraining model parameters such as the strong coupling constant or PDFs.

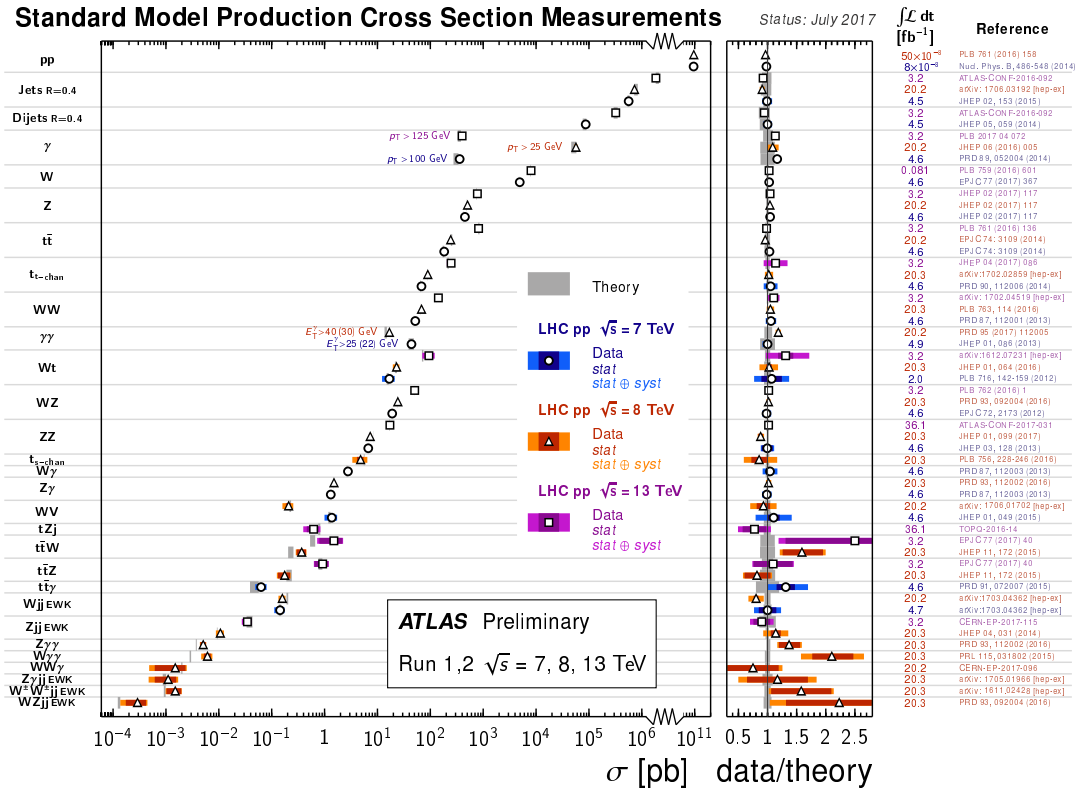

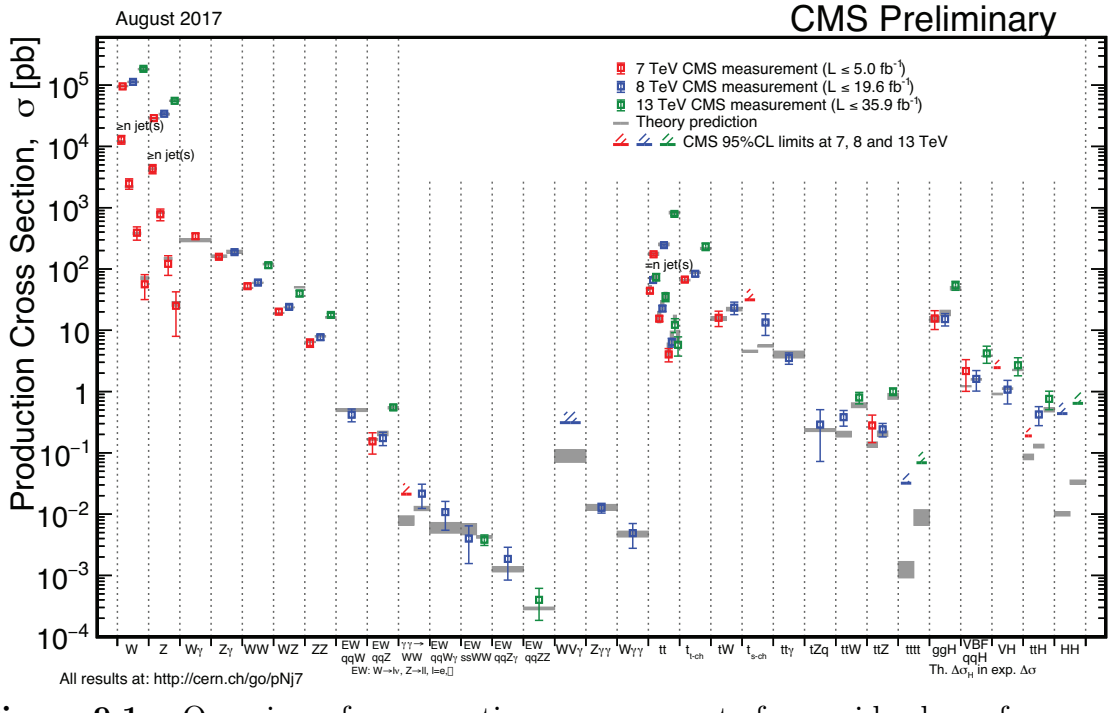

Figure 9.1: Overview of cross section measurements for a wide class of processes and observables, as obtained by the ATLAS [309] and CMS [310] experiments at the LHC, for centre-of-mass energies of 7, 8 and 13 TeV. Also shown are the theoretical predictions and their uncertainties.

Among the most important cross sections measured is the inclusive jet spectrum as a function of the jet transverse energy (E_t) or the jet transverse momentum (p_t), for several rapidity regions and for p_t up to 700 GeV at the Tevatron and ~ 2 TeV at the LHC. It is worth noting that this upper limit in p_t corresponds to a distance scale of $\sim 10^{-19}$ m: no other experiment so far is able to directly probe smaller distance scales of nature than this measurement. Whereas the Tevatron measurements (Refs. 311–313) were based on the infrared- and collinear-safe k_t algorithm in addition to the more widely used Midpoint and JetCLU algorithms of the past, the LHC experiments focus on the *anti-k_t* algorithm using various radius parameters. Measurements by ALICE, ATLAS and CMS have been published in Refs. 314–321. Reviews can be found in, *e.g.*, Refs. 283,322,323.

In general we observe a good description of the data by the NLO QCD predictions, over about 11 orders of magnitude in cross section. The experimental systematic uncertainties are dominated by the jet energy scale uncertainty, quoted to be in the range of a few percent (see for instance the review in Ref. 324), leading to uncertainties of $\sim 5-30\%$ on the cross section, increasing with p_t and rapidity. The PDF uncertainties dominate the theoretical uncertainty at large p_t and rapidity. In fact, inclusive jet data are important inputs to global PDF fits (see [325] for a recent review). Constraints on the PDFs can also be obtained from ratios of inclusive cross sections at different center-of-mass energies [315,320]. In general, ratios of jet cross sections are a means to (at least partially) cancel the jet energy scale uncertainties and thus provide jet observables with significantly improved precision.

Dijet events are analyzed in terms of their invariant mass and angular distributions, which allows for tests of NLO QCD predictions (see *e.g.* Refs. [319,326,327] for recent LHC results), and setting stringent limits on deviations from the Standard Model, such as quark compositeness or contact interactions (some examples can be found in Refs. 328–334). Furthermore, dijet azimuthal correlations between the two leading jets, normalized to the total dijet cross section, are an extremely valuable tool for studying the spectrum of gluon radiation in the event. The azimuthal separation of the two leading jets is sensitive to multi-jet production, avoiding at the same time large systematic uncertainties from the jet energy calibration. For example, results from the Tevatron [335,336] and the LHC [337–339] show that the LO (non-trivial) prediction for this observable, with at most three partons in the final state, is not able to describe the data for an azimuthal separation below $2\pi/3$, where NLO contributions (with 4 partons) restore the agreement with data. In addition, this observable can be employed to tune Monte Carlo predictions of soft gluon radiation.

Further examples of dijet observables that probe special corners of phase space are those which involve forward (large rapidity) jets and where a large rapidity separation, possibly also a rapidity gap, is required between the two jets. Reviews of such measurements can be found in Refs. [283,340], showing that no single prediction is capable of describing the data in all phase-space regions. In particular, no conclusive evidence for BFKL effects in these observables has been established so far.

Beyond dijet final states, measurements of the production of three or more jets, including cross section ratios, have been performed (see Refs. [283,341] for recent reviews), as a means of testing perturbative QCD predictions, determining the strong coupling

constant (at NLO precision so far), and probing/tuning MC models, in particular those combining multi-parton matrix elements with parton showers.

In terms of precision achieved, measurements of inclusive vector boson (W, Z) production outperform the jet studies described above and provide the most precisely determined observables at hadron colliders so far. This is because the experimental signatures are based on leptons that are measured much more accurately than jets. At the LHC [342–348], the dominant uncertainty stems from the luminosity determination (∼2–4%), while other uncertainties (*e.g.* statistics, lepton efficiencies) are controlled at the 1–3% level. The uncertainty from the acceptance correction of about 1–2% can be reduced by measuring so-called fiducial cross sections, ie. by applying kinematic cuts also to the particle level of the theoretical predictions. A further reduction or even complete elimination of particular uncertainties (*e.g.* luminosity) is achieved by measuring cross section ratios (W/Z or W^+/W^-) or differential distributions that are normalised to the inclusive cross section. On the theory side, as discussed earlier in this review, the production of these color-singlet states has been calculated up to NNLO accuracy. Since the dominant theoretical uncertainty is related to the choice of PDFs, these high-precision data provide useful handles for PDF determinations.

Further insights are obtained from measurements of differential vector boson production, as a function of the invariant dilepton mass, the boson's rapidity or its transverse momentum. For example, the dilepton invariant mass distribution has been measured [349–353] for masses between 15 and 2000 GeV, covering more than 8 orders of magnitude in cross section. NNLO QCD predictions, together with modern PDF sets and including higher-order electroweak and QED final-state radiation corrections, describe the data to within 5–10% over this large range, whereas NLO predictions show larger deviations, unless matched to a parton shower.

Similar conclusions can be drawn from the observed rapidity distribution of the dilepton system (see *e.g.* [342,350]) or, in the case of W production, from the observed charged lepton rapidity distribution and its charge asymmetry. The latter is particularly sensitive to differences among PDF sets [342,354,355], also thanks to the high precision achieved by the ATLAS and CMS experiments for central rapidity ranges. These measurements are nicely extended to the very forward region, up to 4.5 in lepton rapidity, by the LHCb experiment.

An overview of this kind of measurements can be found in Ref. 283. There one can also find a discussion of and references to LHC results from studies of the vector boson's transverse momentum distribution, p_t^V (see also Refs. 356,357). This observable probes different aspects of higher-order QCD effects and is sensitive to jet production in association to the vector boson, without suffering from the large jet energy scale uncertainties since there is no explicit jet reconstruction. Whereas in the p_t^V region of several tens to hundreds of GeV the NNLO predictions (that effectively are of NLO accuracy for this variable) agree with the data to within about 10%, at transverse momentum below ∼5–10 GeV the fixed order predictions fail and soft-gluon resummation is needed to restore the agreement with data. Correspondingly, MC models implementing parton shower matching to LO or NLO matrix elements provide good predictions at low and intermediate p_t^V, but deviate up to 40% at high p_t^V.

While in principle inclusive and differential photon production represents a similar tool for studying effects as described above, the experimental results are less precise than for W and Z production, related to the greater challenges encountered in photon reconstruction and purity determination compared to lepton final states.

In terms of complexity, probably the most challenging class of processes is vector boson (photon, W, Z) production together with jets. By now the amount of results obtained both at the Tevatron and at the LHC is so extensive that a comprehensive discussion with a complete citation list would go much beyond the scope of this *Review*. We rather refer to recent summaries in Refs. 283,358 and to previous versions of this *Review*.

The measurements cover a very large phase space, *e.g.* with jet transverse momenta between 30 GeV and $\sim$ 800 GeV and jet rapidities up to $|y| < 4.4$. Jet multiplicities as high as seven jets accompanying the vector boson have already been probed at the LHC, together with a substantial number of other kinematical observables, such as angular correlations among the various jets or among the jets and the vector boson, or the sum of jet transverse momenta, H_T. Whereas the jet p_t and H_T distributions are dominated by jet energy scale uncertainties at levels similar to those discussed above for inclusive jet production, angular correlations and jet multiplicity ratios have been measured with a precision of $\sim 10\%$, see *e.g.* Refs. 359,275.

A general observation is that MC models, which implement a matching of matrix-element calculations with parton showers, provide a good description of the data within uncertainties. Also NLO calculations for up to five jets [122] in addition to the vector boson are in good agreement with the data over that phase space, where the calculations are applicable; that is, one can not expect such predictions to work for, eg., the p_t distribution of the $n+1$st jet with $V+n$ jets calculated at NLO. However, with the high statistics available to and the high precision achieved by the LHC experiments, some more detailed observations can be made. MC models that implement parton shower matching to LO matrix elements (LO+PS) tend to overpredict the data at large jet and/or boson p_t, while parton shower matching to NLO matrix elements gives better agreement. These problems of LO+PS models are less acute when looking at angular correlations.

Also, electroweak corrections are expected to become more and more relevant now that the TeV energy range starts to be explored. For example, such corrections were found [360] to be sizeable (tens of percent) when studying the ratio $(d\sigma^{\gamma}/dp_t)/(d\sigma^{Z}/dp_t)$ in $\gamma\,(Z)$+jet production, p_t being the boson's transverse momentum, and might account for (some of) the differences observed in a CMS measurement [361] of this quantity.

The challenges get even more severe in the case of vector boson plus heavy quark (b, c) production, both because of theoretical issues (an additional scale is introduced by the heavy quark mass and different schemes exist for the handling of heavy quarks and their mass effects in the initial and/or final state) and because of additional experimental uncertainties related to the heavy-flavour tagging. A review of heavy quark production at the LHC can be found in Ref. 362. There it is stated that studies of b-jet production with or without associated W and Z bosons reveal the di-b-jet p_t and mass spectra to be well modelled, within experimental and theoretical uncertainties, by most generators on the market. However, sizeable differences between data and predictions are seen in the modelling of events with single b jets, particularly at large b-jet p_t, where gluon splitting

processes become dominant, as also confirmed by studies of b-hadron and b-jet angular correlations.

A number of interesting developments, in terms of probing higher-order QCD effects, have occurred in the sector of diboson production, in particular for the WW and $\gamma\gamma$ cases. Regarding the former, an early disagreement of about 10% between the LHC measurements and the NLO predictions had led to a number of speculations of possible new physics effects in this channel. However, more recent ATLAS and CMS measurements [363–365] are in agreement with the NNLO prediction [68].

In the case of diphoton production, ATLAS [366,367] and CMS [368] have provided accurate measurements, in particular for phase-space regions that are sensitive to radiative QCD corrections (multi-jet production), such as small azimuthal photon separation. While there are large deviations between data and NLO predictions in this region, a calculation [147] at NNLO accuracy manages to mostly fill this gap. This is an interesting example where scale variations can not provide a reliable estimate of missing contributions beyond NLO, since at NNLO new channels appear in the initial state (gluon fusion in this case).

In terms of heaviest particle involved, top-quark production at the LHC has become an important tool for probing higher-order QCD calculations, thanks to very impressive achievements both on the experimental and theoretical side, as extensively summarised in Ref. 369. Regarding $t\bar{t}$ production, the most precise inclusive cross section measurements are achieved using the dilepton ($e\,\mu$) final state, with a total uncertainty of 4%. This is of about the same size as the uncertainty on the most advanced theoretical prediction [67], obtained at NNLO with additional soft-gluon resummation at NNLL accuracy. There is excellent agreement between data and QCD prediction.

A large number of differential cross section measurements have been performed at 7, 8 and 13 TeV centre-of-mass energy, studying distributions such as the top-quark p_t and rapidity, the transverse momentum and invariant mass of the $t\bar{t}$ system (probing scales up to the TeV range), or the number of additional jets. These measurements have been compared to a wide range of predictions, at fixed order up to NNLO as well as using LO or NLO matrix elements matched to parton showers. While in general there is good agreement observed with data, most MC simulations predict a somewhat harder top-quark p_t distribution than seen in data.

Thanks to both the precise measurements of and predictions for the inclusive top-pair cross section, that is sensitive to the strong coupling constant and the top-quark mass, this observable has been used to measure the strong coupling constant at NNLO accuracy from hadron collider data [370,371] (*cf.* Section 9.4 below), as well as to obtain a measurement of the top-quark's pole mass without employing direct reconstruction methods [370,372,373].

Finally, it is worth mentioning that steps are being undertaken towards using the newly found Higgs boson as a new tool for QCD studies, since Higgs production, dominated by the gluon fusion process, is subject to very large QCD corrections. First studies of fiducial and differential cross sections, using the ZZ, $\gamma\gamma$ and WW decay channels, have already been performed [374–380], and the current experimental precision of $\sim 20\%$ or

more is expected to be substantially reduced with the future LHC data.

9.4. Determinations of the strong coupling constant

Beside the quark masses, the only free parameter in the QCD Lagrangian is the strong coupling constant α_s. The coupling constant in itself is not a physical observable, but rather a quantity defined in the context of perturbation theory, which enters predictions for experimentally measurable observables, such as R in Eq. (9.7).

Here, we retain the 2016 summary [381] of measurements of α_s and extraction of the world average value of $\alpha_s(M_Z^2)$, and leave an update of this section to a later version of *this Review* ♯. This is done because only very few new results satisfying the selection criteria defined below were available at the deadline for *this Review*, while further new results are expected to arrive (and actually have arrived) past-deadline.

Many experimental observables are used to determine α_s. Considerations in such determinations include:

- The observable's sensitivity to α_s as compared to the experimental precision. For example, for the e^+e^- cross section to hadrons (*cf.* R in Sec. 9.2.1), QCD effects are only a small correction, since the perturbative series starts at order α_s^0; 3-jet production or event shapes in e^+e^- annihilations are directly sensitive to α_s since they start at order α_s; the hadronic decay width of heavy quarkonia, $\Gamma(\Upsilon \to \text{hadrons})$, is very sensitive to α_s since its leading order term is $\propto \alpha_s^3$.
- The accuracy of the perturbative prediction, or equivalently of the relation between α_s and the value of the observable. The minimal requirement is generally considered to be an NLO prediction. Some observables are predicted to NNLO (many inclusive observables, 3-jet rates and event shapes in e^+e^- collisions) or even N^{3}LO (e^+e^- hadronic cross section and τ branching fraction to hadrons). In certain cases, fixed-order predictions are supplemented with resummation. The precise magnitude of theory uncertainties is usually estimated as discussed in Sec. 9.2.4.
- The size of non-perturbative effects. Sufficiently inclusive quantities, like the e^+e^- cross section to hadrons, have small non-perturbative contributions $\sim \Lambda^4/Q^4$. Others, such as event-shape distributions, have contributions $\sim \Lambda/Q$.
- The scale at which the measurement is performed. An uncertainty δ on a measurement of $\alpha_s(Q^2)$, at a scale Q, translates to an uncertainty $\delta' = (\alpha_s^2(M_Z^2)/\alpha_s^2(Q^2)) \cdot \delta$ on $\alpha_s(M_Z^2)$. For example, this enhances the already important impact of precise low-Q measurements, such as from τ decays, in combinations performed at the M_Z scale.

The selection of results from which to determine the world average value of $\alpha_s(M_Z^2)$ is restricted to those which are

- published in a peer-reviewed journal,
- based on the most complete perturbative QCD predictions, *i.e.* to those using NNLO or higher-order expansions.

♯ The time evolution of α_s combinations can be followed by consulting Refs. [383–385] as well as earlier editions of *this Review*.

This excludes *e.g.* results from jet production in DIS at HERA and at hadron colliders which are based on calculations at NLO only. These will nevertheless be discussed in this review, as they are important ingredients for the experimental evidence of the energy dependence of α_s, *i.e.* for Asymptotic Freedom, one of the key features of QCD. Note that results which do not include reliable estimates of experimental, systematic and theoretical uncertainties, which are based on not commonly accepted procedures like scale optimization, or which omit discussion or accounting of non-perturbative corrections and effects, will not be referenced at all in this review.

In order to calculate the world average value of $\alpha_s(M_Z^2)$, we apply an intermediate step of pre-averaging results within certain sub-fields like e^+e^- annihilation, DIS and hadronic τ-decays, and calculate the overall world average from those pre-averages rather than from individual measurements. This is done because in most sub-fields one observes that different determinations of the strong coupling from substantially similar datasets lead to values of α_s that are only marginally compatible with each other, or with the final world average value, which presumably is a reflection of the challenges of evaluating and including appropriate systematic uncertainties.

So for each sub-field, the *unweighted average* of all selected results is taken as the pre-average value of $\alpha_s(M_Z^2)$, and the unweighted average of the quoted uncertainties is assigned to be the respective overall error of this pre-average. However, if this error appears to be smaller than the unweighted standard deviation - i.e. the *spread* - of the results, the standard deviation is taken as the overall uncertainty instead. This is done in order to arrive at an unbiased estimator of the average value of $\alpha_s(M_Z^2)$ from this sub-field, and to avoid that singular, optimistic estimates of systematic uncertainties dominate the field if these are not backed up by a broader consensus [†].

Assuming that the resulting pre-averages are largely independent of each other, we determine the final world average value using the method of 'χ^2 *averaging*', as proposed, *e.g.*, in Ref. 386, in order to treat cases of possible (unknown) correlations as well as possibly underestimated systematic uncertainties in a meaningful and well defined manner: the central value is determined as the weighted average of the different input values. An initial uncertainty of the central value is determined treating the uncertainties of all individual measurements as being uncorrelated and of Gaussian nature, and the overall χ^2 to the central value is calculated. If this initial χ^2 is larger than the number of degrees of freedom, then all individual uncertainties are enlarged by a common factor such that χ^2/d.o.f. equals unity. If the initial value of χ^2 is smaller than the number of degrees of freedom, an overall correlation coefficient is introduced and determined by requiring that the total χ^2/d.o.f. equals unity. In both cases, the resulting overall uncertainty of α_s is larger than the initial estimate of the uncertainty.

[†] In most practical cases, this procedure arrives at similar values as obtained from the '*range averaging*' method which we used in previous *Reviews*, while it avoids potential shortcomings and biases of the latter.

9.4.1. ***Hadronic τ decays*** :
Based on complete N^{3}LO predictions [35], analyses of the τ hadronic decay width and spectral functions have been performed, leading to precise determinations of α_s at the energy scale of M_τ^2 [35,387–393]. They are based on different approaches to treat perturbative and non-perturbative contributions, the impacts of which are a matter of intense discussions, see *e.g.* [391] and [394].

In particular, there is a significant difference between results obtained using fixed-order (FOPT) or contour improved perturbation theory (CIPT), such that analyses based on CIPT generally arrive at about 7% larger values of $\alpha_s(M_\tau^2)$ than those based on FOPT. When converted to $\alpha_s(M_Z^2)$, the difference is about 2%. This uncertainty is about 5 times larger than the typically achieved experimental precision. In addition, most recent results show differences of up to 10% in $\alpha_s(M_\tau^2)$ (3% at M_Z), between different groups using the same data sets and perturbative calculations, most likely due to different treatments of the non-perturbative contributions, c.f. Ref. [393] with Refs. [391,392].

We determine the pre-average value of $\alpha_s(M_Z^2)$ for this sub-field from studies which employ both, FOPT and CIPT expansions, and which include the difference among these in the quoted overall uncertainty: $\alpha_s(M_Z^2) = 0.1202 \pm 0.0019$ [35], $\alpha_s(M_Z^2) = 0.1200 \pm 0.0015$ [391], $\alpha_s(M_Z^2) = 0.1199 \pm 0.0015$ [392], and $\alpha_s(M_Z^2) = 0.1165 \pm 0.0019$ [393].

We also include the result from τ decay and lifetime measurements, obtained in Sec. *Electroweak Model and constraints on New Physics* of the 2013 edition of this *Review*, $\alpha_s(M_Z^2) = 0.1193 \pm 0.0023$. All these are summarised in Fig. 9.2. Determining the unweighted average of the central values and their overall uncertainties, we arrive at $\alpha_s(M_Z^2) = 0.1192 \pm 0.0018$ which we will use as the first input for determining the world average value of $\alpha_s(M_Z^2)$. This corresponds to $\alpha_s(M_\tau^2) = 0.325 \pm 0.015$ at the scale of the τ-mass.

9.4.2. ***Lattice QCD*** :
There are several current results on α_s from lattice QCD, see also Sec. *Lattice QCD* in this *Review*. The HPQCD collaboration [395] computes Wilson loops and similar short-distance quantities with lattice QCD and analyzes them with NNLO perturbative QCD. This yields a value for α_s, but the lattice scale must be related to a physical energy/momentum scale. This is achieved with the Υ'-Υ mass difference, however, many other quantities could be used as well [396]. HPQCD obtains $\alpha_s(M_Z^2) = 0.1184 \pm 0.0006$, where the uncertainty includes effects from truncating perturbation theory, finite lattice spacing and extrapolation of lattice data. An independent perturbative analysis of a subset of the same lattice-QCD data yields $\alpha_s(M_Z^2) = 0.1192 \pm 0.0011$ [397]. Using another, independent methodology, the current-current correlator method, HPQCD obtains $\alpha_s(M_Z^2) = 0.1182 \pm 0.0007$ [395,398]. The analysis of Ref. 399, which uses the Schroedinger functional scheme and avoids the staggered fermion treatment of Ref. 395, finds $\alpha_s(M_Z^2) = 0.1205 \pm 0.0008 \pm 0.0005\,^{+0.0000}_{-0.0017}$, where the first uncertainty is statistical and the others are from systematics. Since this approach uses a different discretization of lattice fermions and a different general methodology, it provides an independent cross check of other lattice extractions of α_s. A study of the ETM collaboration [400] used lattice data with u, d, s and c quarks in the sea and examined the

ghost-gluon coupling, obtaining $\alpha_s(M_Z^2) = 0.1196 \pm 0.0012$. Finally, a determination of α_s from the QCD static potential [401] results in $\alpha_s(M_Z^2) = 0.1166^{+0.0012}_{-0.0008}$. The JLQCD collaboration, in an analysis of Adler functions, has recently corrected their initial result of $\alpha_s(M_Z^2) = 0.1181^{+0.0014}_{-0.0012}$ downwards, by more than 5 standard deviations of their assigned uncertainty, to $\alpha_s(M_Z^2) = 0.1118^{+0.0016}_{-0.0017}$ [402]. For this and other reasons discussed in [403], we do not include this result in our determination of the average lattice result.

A summary of the results discussed above is given in Fig. 9.2. They average, applying the method of taking the unweighted averages of the central values and their quoted uncertainties at face value, to $\alpha_s(M_Z^2) = 0.1188 \pm 0.0011$, which we take as our second result for the determination of the world average value of α_s. This compares well to a similar compilation and summary provided by the FLAG Working Group [403], suggesting $\alpha_s(M_Z^2) = 0.1184 \pm 0.0012$ as the overall average of lattice determinations of α_s. Both these error estimates are more conservative than the one (± 0.0005) we used in our previous *Review* where we applied the χ^2 *averaging* method.

9.4.3. ***Deep inelastic lepton-nucleon scattering (DIS)*** :
Studies of DIS final states have led to a number of precise determinations of α_s: a combination [404] of precision measurements at HERA, based on NLO fits to inclusive jet cross sections in neutral current DIS at high Q^2, provides combined values of α_s at different energy scales Q, as shown in Fig. 9.3, and quotes a combined result of $\alpha_s(M_Z^2) = 0.1198 \pm 0.0032$. A more recent study of multijet production [405], based on improved reconstruction and data calibration, confirms the general picture, albeit with a somewhat smaller value of $\alpha_s(M_Z^2) = 0.1165 \pm 0.0039$, still in NLO. An evaluation of inclusive jet production, including *approximate* NNLO contributions [406], reduces the theoretical prediction for jet production in DIS, improves the description of the final HERA data in particular at high photon virtuality Q^2 and increases the central fit value of the strong coupling constant.

Another class of studies, analyzing structure functions in NNLO QCD (and partly beyond), provide results which serve as relevant inputs for the world average of α_s. Most of these studies do *not*, however, explicitly include estimates of theoretical uncertainties when quoting fit results of α_s. In such cases we add, in quadrature, half of the difference between the results obtained in NNLO and NLO to the quoted errors: A combined analysis of non-singlet structure functions from DIS [407], based on QCD predictions up to N^{3}LO in some of its parts, results in $\alpha_s(M_Z^2) = 0.1141 \pm 0.0022$ (BBG). Studies of singlet and non-singlet structure functions, based on NNLO predictions, result in $\alpha_s(M_Z^2) = 0.1134 \pm 0.0025$ [408] (ABM) and in $\alpha_s(M_Z^2) = 0.1158 \pm 0.0036$ [409] (JR). The MSTW group [410], also including data on jet production at the Tevatron, obtains, at NNLO[##], $\alpha_s(M_Z^2) = 0.1171 \pm 0.0024$. A recent update of this analysis, also including hadron collider data, determined a new set of parton density functions (MMHT2014) [411], together with $\alpha_s(M_Z^2) = 0.1172 \pm 0.0013$. The NNPDF group [412]

[##] Note that for jet production at a hadron collider, only NLO predictions are available, while for the structure functions full NNLO was utilized.

presented a result, $\alpha_s(M_Z^2) = 0.1173 \pm 0.0011$, which is in line with the one from the MMHT group, including rather small experimental and theoretical uncertainties of only 6 and 9 per-mille, respectively.

We note that criticism has been expressed on some of the above extractions. Among the issues raised, we mention the neglect of singlet contributions at $x \geq 0.3$ in pure non-singlet fits [413], the impact and detailed treatment of particular classes of data in the fits [413,414], possible biases due to insufficiently flexible parametrizations of the PDFs [415] and the use of a fixed-flavor number scheme [416,417].

Summarizing the results from world data on structure functions, taking the *unweighted average* of the central values and errors of all selected results, leads to a pre-average value of $\alpha_s(M_Z^2) = 0.1156 \pm 0.0021$, see Fig. 9.2.

9.4.4. ***Heavy quarkonia decays*** :
The latest extraction of the strong coupling constant from an analysis of radiative Υ decays [418] resulted in $\alpha_s(M_Z^2) = 0.119^{+0.006}_{-0.005}$. This determination is based on QCD at NLO only, so it will not be considered for the final extraction of the world average value of α_s; it is, however, an important ingredient for the demonstration of Asymptotic Freedom as given in Fig. 9.3.

9.4.5. ***Hadronic final states of e^+e^- annihilations*** :
Re-analyses of event shapes in e^+e^- annihilation, measured around the Z peak and at LEP2 center-of-mass energies up to 209 GeV, using NNLO predictions matched to NLL resummation and Monte Carlo models to correct for hadronization effects, resulted in $\alpha_s(M_Z^2) = 0.1224 \pm 0.0039$ (ALEPH) [419], with a dominant theoretical uncertainty of 0.0035, and in $\alpha_s(M_Z^2) = 0.1189 \pm 0.0043$ (OPAL) [420]. Similarly, an analysis of JADE data [421] at center-of-mass energies between 14 and 46 GeV gives $\alpha_s(M_Z^2) = 0.1172 \pm 0.0051$, with contributions from hadronization model and from perturbative QCD uncertainties of 0.0035 and 0.0030, respectively. Precise determinations of α_s from 3-jet production alone, in NNLO, resulted in $\alpha_s(M_Z^2) = 0.1175 \pm 0.0025$ [422] from ALEPH data and in $\alpha_s(M_Z^2) = 0.1199 \pm 0.0059$ [423] from JADE. These results are summarized in the upper half of the e^+e^- sector of Fig. 9.2.

Another class of α_s determinations is based on analytic calculations of non-perturbative and hadronization effects, rather than on Monte Carlo models [424–427], using methods like power corrections, factorization of soft-collinear effective field theory, dispersive models and low scale QCD effective couplings. In these studies, the world data on Thrust distributions, or - most recently - C-parameter distributions, are analysed and fitted to perturbative QCD predictions in NNLO matched with resummation of leading logs up to N^{3}LL accuracy, see Sec. 9.2.3.3. The results are $\alpha_s(M_Z^2) = 0.1164^{+0.0028}_{-0.0024}$ [424], $\alpha_s(M_Z^2) = 0.1135 \pm 0.0011$ [425] and $\alpha_s(M_Z^2) = 0.1137^{+0.0034}_{-0.0027}$ [426] from Thrust, and $\alpha_s(M_Z^2) = 0.1123 \pm 0.0015$ [427] from C-parameter. They are also displayed in Fig. 9.2.

Not to be included in the computation of the world average but worth mentioning are a computation of the NLO corrections to 5-jet production and comparison to the measured 5-jet rates at LEP [428], giving $\alpha_s(M_Z^2) = 0.1156^{+0.0041}_{-0.0034}$, and a computation of non-perturbative and perturbative QCD contributions to the scale

evolution of quark and gluon jet multiplicities, including resummation, resulting in $\alpha_s(M_Z^2) = 0.1199 \pm 0.0026$ [429].

We note that there is criticism on both classes of α_s extractions described above: those based on corrections of non-perturbative hadronization effects using QCD-inspired Monte Carlo generators (since the parton level of a Monte Carlo simulation is not defined in a manner equivalent to that of a fixed-order calculation), as well as studies based on non-perturbative analytic calculations, as their systematics have not yet been fully verified. In particular, quoting rather small overall experimental, hadronization and theoretical uncertainties of only 2, 5 and 9 per-mille, respectively [425,427], seems unrealistic and has neither been met nor supported by other authors or groups.

In view of these open questions, the determination of the *unweighted average* and uncertainties is supposed to provide the most appropriate and unbiased estimate of the average value of $\alpha_s(M_Z^2)$ for this sub-field, which results in $\alpha_s(M_Z^2) = 0.1169 \pm 0.0034$.

9.4.6. ***Hadron collider results*** :
Significant determinations of α_s from data at hadron colliders, *i.e.* the Tevatron and the LHC, are obtained, however mostly still limited to QCD at NLO. At $\sqrt{s} = 1.96$ TeV,

$$\alpha_s(M_Z^2) = 0.1161^{+0.0041}_{-0.0048} \text{ and}$$
$$\alpha_s(M_Z^2) = 0.1191^{+0.0048}_{-0.0071}$$

result from studies of inclusive jet cross sections [430] and from jet angular correlations [431], respectively. ATLAS data on inclusive jet production at $\sqrt{s} = 7$ TeV [432] lead to [433]

$$\alpha_s(M_Z^2) = 0.1151^{+0.0093}_{-0.0087} \, .$$

Here, experimental systematics, the choice of jet scale and the use of different PDFs dominate the large overall uncertainties. Determinations of α_s from CMS data on the ratio of inclusive 3-jet to 2-jet cross sections [434], from inclusive jet production [435] and from the 3-jet differential cross section [436] quoted values of

$$\alpha_s(M_Z^2) = 0.1148 \pm 0.0014(\text{exp.})^{+0.0053}_{-0.0023}(\text{theo.}) \, ,$$
$$\alpha_s(M_Z^2) = 0.1185 \pm 0.0019(\text{exp.})^{+0.0060}_{-0.0037}(\text{theo.}) \text{ and}$$
$$\alpha_s(M_Z^2) = 0.1171 \pm 0.0013(\text{exp.})^{+0.0073}_{-0.0047}(\text{theo.}) \, ,$$

respectively. Most recently, the ATLAS collaboration reported

$$\alpha_s(M_Z^2) = 0.1173 \pm 0.0010(\text{exp.})^{+0.0065}_{-0.0026}(\text{theo.}) \text{ and}$$
$$\alpha_s(M_Z^2) = 0.1195 \pm 0.0018(\text{exp.})^{+0.0062}_{-0.0022}(\text{theo.})$$

using the transverse energy-energy correlation function (TEEC) and its associated azimuthal asymmetry (ATEEC), respectively [271]. All these results are at NLO only, however they provide valuable new values of α_s at energy scales now extending up to 1.4 TeV. Although not contributing to the overall world average of α_s which we determine

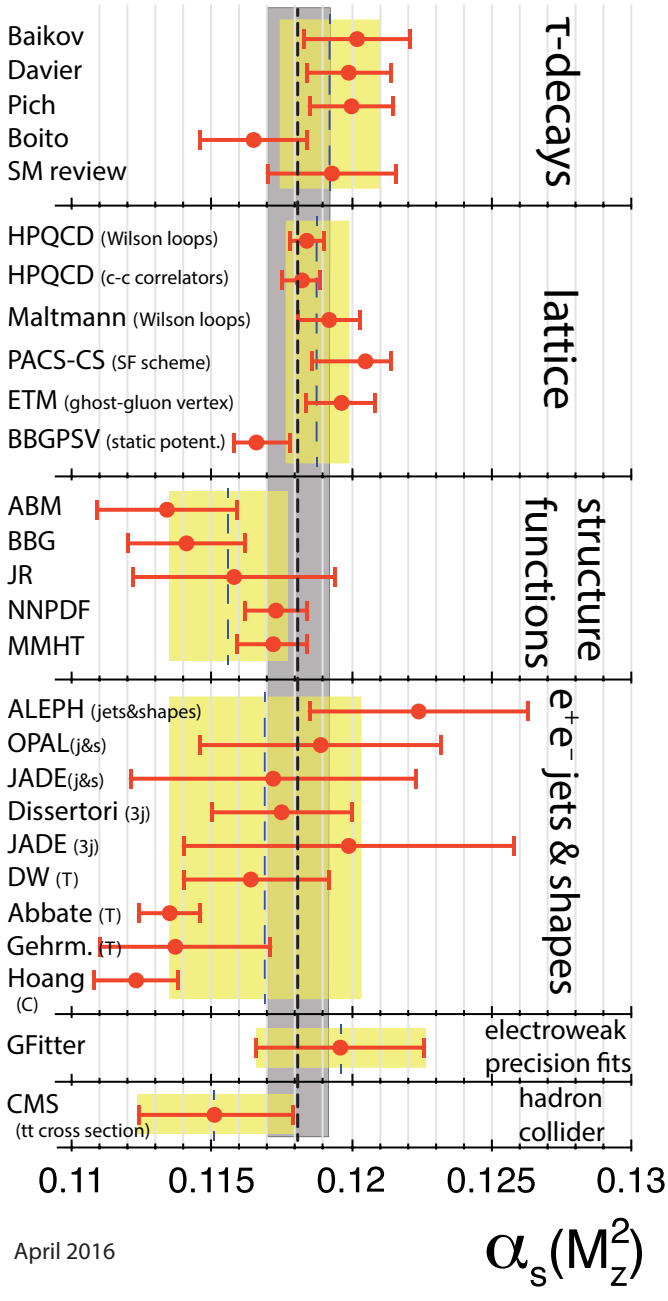

Figure 9.2: Summary of determinations of $\alpha_s(M_Z^2)$ from the six sub-fields discussed in the text. The yellow (light shaded) bands and dashed lines indicate the pre-average values of each sub-field. The dotted line and grey (dark shaded) band represent the final world average value of $\alpha_s(M_Z^2)$.

below, it may be worth mentioning that the collider results listed above average to a value of $\alpha_s(M_Z^2) = 0.1172 \pm 0.0059$.

So far, only one analysis is available which involves the determination of α_s from

hadron collider data in NNLO of QCD: from a measurement of the $t\bar{t}$ cross section at $\sqrt{s} = 7$ TeV, CMS [370] determined

$$\alpha_s(M_Z^2) = 0.1151^{+0.0028}_{-0.0027} \ ,$$

whereby the dominating contributions to the overall error are experimental ($^{+0.0017}_{-0.0018}$), from parton density functions ($^{+0.0013}_{-0.0011}$) and the value of the top quark pole mass (± 0.0013).

This latter result will enter our determination of the new world average of α_s, and will thereby open a new sub-field of α_s determinations in this *Review*. We note, however, that so far there is only this one result in this sub-field. While there are more recent measurements of $t\bar{t}$ cross sections from ATLAS and from CMS, at $\sqrt{s} = 7$, 8 and at 13 TeV, none quotes further extractions of α_s. A more reliable result will thus be left to the next *Review*, however we note that the most recent measurements of $t\bar{t}$ cross sections imply larger values of $\alpha_s(M_Z^2)$ than the one which we use, at this time, as result for this sub-field.

9.4.7. *Electroweak precision fit* :

The N^{3}LO calculation of the hadronic Z decay width [35] was used in the latest update of the global fit to electroweak precision data [437], resulting in

$$\alpha_s(M_Z^2) = 0.1196 \pm 0.0030 \ ,$$

claiming a negligible theoretical uncertainty. We note that results from electroweak precision data, however, strongly depend on the strict validity of Standard Model predictions and the existence of the minimal Higgs mechanism to implement electroweak symmetry breaking. Any - even small - deviation of nature from this model could strongly influence this extraction of α_s.

9.4.8. *Determination of the world average value of* $\alpha_s(M_Z^2)$:

Obtaining a world average value for $\alpha_s(M_Z^2)$ is a non-trivial exercise. A certain arbitrariness and subjective component is inevitable because of the choice of measurements to be included in the average, the treatment of (non-Gaussian) systematic uncertainties of mostly theoretical nature, as well as the treatment of correlations among the various inputs, of theoretical as well as experimental origin.

We have chosen to determine pre-averages for sub-fields of measurements which are considered to exhibit a maximum of independence between each other, considering experimental as well as theoretical issues. The six pre-averages are summarized in Fig. 9.2. We recall that these are exclusively obtained from extractions which are based on (at least) full NNLO QCD predictions, and are published in peer-reviewed journals at the time of completing this *Review*. These pre-averages are then combined to the final world average value of $\alpha_s(M_Z^2)$, using the χ^2 *averaging method* and error treatment as described above. From these, we determine the new world average value of

$$\alpha_s(M_Z^2) = 0.1181 \pm 0.0011 \ , \tag{9.23}$$

with an uncertainty of 0.9 %.*** This world average value is in reasonable agreement with that from the 2013 version of this *Review*, which was $\alpha_s(M_Z^2) = 0.1185 \pm 0.0006$, however at a somewhat decreased central value and with an overall uncertainty that has almost doubled. These changes are mainly due to the following developments:

- the uncertainty of the combined lattice result, now using the same averaging procedure as applied to the other sub-fields, is more conservative than that used in our previous *Review*, leading to a larger final uncertainty of the new world average, and to a reduced fixing power towards the central average value;
- the relatively low value of α_s from hadron collider results, which currently consists of only one measurement of the $t\bar{t}$ cross section at $\sqrt{s} = 7$ TeV [370] that is likely to be a fluctuation to the low side.

For convenience, we also provide the values for $\Lambda_{\overline{MS}}$ which correspond to the new world average:

$$\Lambda_{\overline{MS}}^{(6)} = (89 \pm 6) \text{ MeV}, \tag{9.24a}$$
$$\Lambda_{\overline{MS}}^{(5)} = (210 \pm 14) \text{ MeV}, \tag{9.24b}$$
$$\Lambda_{\overline{MS}}^{(4)} = (292 \pm 16) \text{ MeV}, \tag{9.24c}$$
$$\Lambda_{\overline{MS}}^{(3)} = (332 \pm 17) \text{ MeV}, \tag{9.24d}$$

for $n_f = 6$, 5, 4 and 3 quark flavors, which are determined using the 4-loop expression for the running of α_s according to Eq. (9.5) and 3-loop matching at the charm-, bottom- and top-quark pole masses of 1.3, 4.2 and 173 GeV/c^2, respectively. Note that for scales below a few GeV, Eq. (9.5) starts to differ significantly from the exact solution of the renormalization group equation Eq. (9.3) and the latter is then to be preferred.

In order to further test and verify the sensitivity of the new average value of $\alpha_s(M_Z^2)$ to the different pre-averages and fields of α_s determinations, we give each of the averages obtained when leaving out one of the six input values, as well as the respective, initial value of χ^2 :

$$\alpha_s(M_Z^2) = 0.1179 \pm 0.0011 \quad (\text{w/o } \tau \text{ results; } \chi_0^2/\text{d.o.f.} = 3.3/4), \tag{9.25a}$$
$$\alpha_s(M_Z^2) = 0.1174 \pm 0.0016 \quad (\text{w/o lattice results; } \chi_0^2/\text{d.o.f.} = 2.9/4), \tag{9.25b}$$
$$\alpha_s(M_Z^2) = 0.1185 \pm 0.0013 \quad (\text{w/o DIS results; } \chi_0^2/\text{d.o.f.} = 2.0/4), \tag{9.25c}$$
$$\alpha_s(M_Z^2) = 0.1182 \pm 0.0010 \quad (\text{w/o } e^+e^- \text{ results; } \chi_0^2/\text{d.o.f.} = 3.5/4), \tag{9.25d}$$
$$\alpha_s(M_Z^2) = 0.1184 \pm 0.0012 \quad (\text{w/o hadron collider; } \chi_0^2/\text{d.o.f.} = 2.4/4) \text{ and} \tag{9.25e}$$
$$\alpha_s(M_Z^2) = 0.1180 \pm 0.0010 \quad (\text{w/o e.w. precision fit; } \chi_0^2/\text{d.o.f.} = 3.4/4). \tag{9.25f}$$

*** The weighted average, treating all inputs as uncorrelated measurements with Gaussian uncertainties, results in $\alpha_s(M_Z^2) = 0.11810 \pm 0.00078$ with $\chi^2/\text{d.o.f.} = 3.7/5$. Requiring $\chi^2/\text{d.o.f.}$ to reach unity calls for an overall correlation factor of 0.28, which increases the overall uncertainty to ± 0.00114.

They are well within the uncertainty of the overall world average quoted above. Note, however, that the average *excluding* the lattice result is no longer as close to the value obtained from lattice alone as was the case in the 2013 *Review*, but is now smaller by almost one standard deviation of its assigned uncertainty.

Notwithstanding the many open issues still present within each of the sub-fields summarised in this *Review*, the wealth of available results provides a rather precise and reasonably stable world average value of $\alpha_s(M_Z^2)$, as well as a clear signature and proof of the energy dependence of α_s, in full agreement with the QCD prediction of Asymptotic Freedom. This is demonstrated in Fig. 9.3, where results of $\alpha_s(Q^2)$ obtained at discrete energy scales Q, now also including those based just on NLO QCD, are summarized. Thanks to the results from the Tevatron and from the LHC, the energy scales at which α_s is determined now extend up to more than 1 TeV[◇].

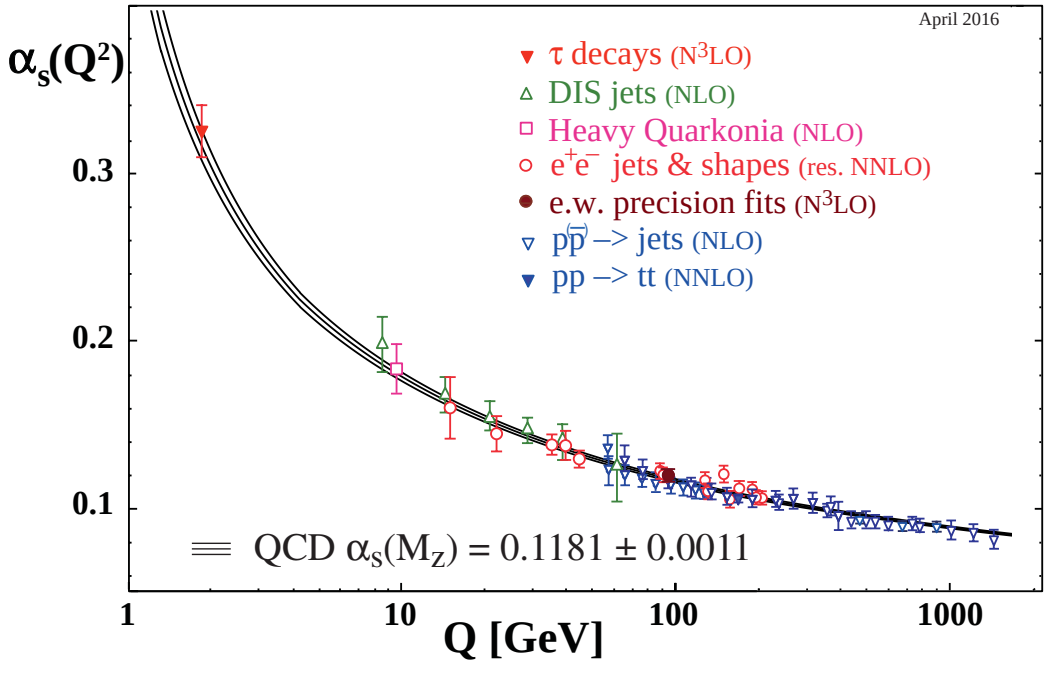

Figure 9.3: Summary of measurements of α_s as a function of the energy scale Q. The respective degree of QCD perturbation theory used in the extraction of α_s is indicated in brackets (NLO: next-to-leading order; NNLO: next-to-next-to leading order; res. NNLO: NNLO matched with resummed next-to-leading logs; N^{3}LO: next-to-NNLO).

◇ We note, however, that in many such studies, like those based on exclusive states of jet multiplicities, the relevant energy scale of the measurement is not uniquely defined. For instance, in studies of the ratio of 3- to 2-jet cross sections at the LHC, the relevant scale was taken to be the average of the transverse momenta of the two leading jets [434], but could alternatively have been chosen to be the transverse momentum of the 3^{rd} jet.

9.5. Acknowledgments

We are grateful to J.-F. Arguin, G. Altarelli, D. Britzger, J. Butterworth, M. Cacciari, L. del Debbio, D. d'Enterria, P. Gambino, C. Glasman Kuguel, N. Glover, M. Grazzini, A. Kronfeld, K. Kousouris, M. Lüscher, Y. Ma, M. d'Onofrio, A. Ramos, S. Sharpe, R. Sommer, G. Sterman, D. Treille, N. Varelas, M. Wobisch, W.M. Yao, C.P. Yuan, and G. Zanderighi for discussions, suggestions and comments on this and earlier versions of this *Review*.

References:

1. R.K. Ellis, W.J. Stirling, and B.R. Webber, *"QCD and collider physics,"* Camb. Monogr. Part. Phys. Nucl. Phys. Cosmol. **81** (1996).
2. C.A. Baker *et al.*, Phys. Rev. Lett. **97**, 131801 (2006).
3. H.-Y. Cheng, Phys. Reports **158**, 1 (1988).
4. G. Dissertori, I.G. Knowles, and M. Schmelling, *"High energy experiments and theory,"* Oxford, UK: Clarendon (2003).
5. R. Brock *et al.*, [CTEQ Collab.], Rev. Mod. Phys. **67**, 157 (1995), see also `http://www.phys.psu.edu/~cteq/handbook/v1.1/handbook.pdf`.
6. A.S. Kronfeld and C. Quigg, Am. J. Phys. **78**, 1081 (2010).
7. T. Plehn, Lect. Notes Phys. **844**, 1 (2012).
8. J. Campbell, J. Huston, F. Krauss *"The Black Book of Quantum Chromodynamics, a Primer for the QCD Era,"* Oxford University Press, UK (2017).
9. R. Stock (Ed.), Relativistic Heavy Ion Physics, Springer-Verlag Berlin, Heidelberg, 2010.
10. *Proceedings of the XXIV International Conference on Ultrarelativistic Nucleus–Nucleus Collisions, Quark Matter 2014*, Nucl. Phys. A, volume 931.
11. R. Hwa and X. N. Wang (Ed.), Quark Gluon Plasma 4, World Scientific Publishing Company, 2010.
12. T. van Ritbergen, J.A.M. Vermaseren, and S.A. Larin, Phys. Lett. **B400**, 379 (1997).
13. M. Czakon, Nucl. Phys. **B710**, 485 (2005).
14. P.A. Baikov, K.G. Chetyrkin, and J.H. Kühn, Phys. Rev. Lett. **118**, 082002 (2017).
15. T. Luthe *et al.*, JHEP **1607**, 127 (2016).
16. F. Herzog *et al.*, JHEP **1702**, 090 (2017).
17. W.A. Bardeen *et al.*, Phys. Rev. **D18**, 3998 (1978).
18. D.J. Gross and F. Wilczek, Phys. Rev. Lett. **30**, 1343 (1973).
19. H.D. Politzer, Phys. Rev. Lett. **30**, 1346 (1973).
20. Y. Schröder and M. Steinhauser, JHEP **0601**, 051 (2006).
21. K.G. Chetyrkin, J.H. Kühn, and C. Sturm, Nucl. Phys. **B744**, 121 (2006).
22. A.G. Grozin *et al.*, JHEP **1109**, 066 (2011).
23. K.G. Chetyrkin, B.A. Kniehl, and M. Steinhauser, Nucl. Phys. **B510**, 61 (1998).
24. M. Dalla Brida *et al.* [ALPHA Collaboration], Phys. Rev. Lett. **117**, 182001 (2016).
25. K.G. Chetyrkin, J.H. Kühn, and M. Steinhauser, Comp. Phys. Comm. **133**, 43 (2000).

26. B. Schmidt and M. Steinhauser, Comp. Phys. Comm. **183**, 1845 (2012) http://www.ttp.kit.edu/Progdata/ttp12/ttp12-02/.
27. F. Herren and M. Steinhauser, arXiv:1703.03751 [hep-ph].
28. A.V. Bednyakov, Phys. Lett. **B741**, 262 (2015).
29. M. Beneke, Phys. Reports **317**, 1 (1999).
30. P. Marquard *et al.*, Phys. Rev. Lett. **114**, 142002 (2015).
31. P.A. Baikov *et al.*, Phys. Lett. **B714**, 62 (2012).
32. K.G. Chetyrkin, J.H. Kühn, and A. Kwiatkowski, Phys. Reports **277**, 189 (1996).
33. Y. Kiyo *et al.*, Nucl. Phys. **B823**, 269 (2009).
34. P.A. Baikov *et al.*, Phys. Rev. Lett. **108**, 222003 (2012).
35. P.A. Baikov, K.G. Chetyrkin, and J.H. Kühn, Phys. Rev. Lett. **101**, 012002 (2008).
36. P.A. Baikov, K.G. Chetyrkin, and J.H. Kühn, Phys. Rev. Lett. **96**, 012003 (2006).
37. P.A. Baikov and K.G. Chetyrkin, Phys. Rev. Lett. **97**, 061803 (2006).
38. F. Herzog *et al.*, JHEP **1708**, 113 (2017).
39. D. Asner *et al.*, arXiv:1307.8265 [hep-ex].
40. H.W. Lin *et al.*, Phys. Rev. **D91**, 054510 (2015);
    C. Alexandrou *et al.*, Phys. Rev. **D92**, 014502 (2015).
41. G. C. Rossi and M. Testa, Phys. Rev. **D96**, 014507 (2017).
42. J. Gao, L. Harland-Lang, and J. Rojo, arXiv:1709.04922 [hep-ph].
43. J. D. Bjorken and E. A. Paschos, Phys. Rev. **185**, 1975 (1969).
44. J.A.M. Vermaseren, A. Vogt, and S. Moch, Nucl. Phys. **B724**, 3 (2005).
45. S. Moch, J.A.M. Vermaseren, and A. Vogt, Nucl. Phys. **B813**, 220 (2009).
46. J. Davies *et al.*, PoS DIS **2016** (2016) 059.
47. E. Laenen *et al.*, Nucl. Phys. **B392**, 162 (1993);
    S. Riemersma, J. Smith, and W.L. van Neerven, Phys. Lett. **B347**, 143 (1995).
48. J. Blümlein, A. De Freitas, and C. Schneider, Nucl. Part. Phys. Proc. **261-262** 185 Nucl. Part. Phys. Proc. **261-262** (2015) 185.
49. J.C. Collins, D.E. Soper, and G.F. Sterman, Adv. Ser. Direct. High Energy Phys. **5**, 1 (1988).
50. J.C. Collins, *Foundations of Perturbative QCD*, Cambridge University Press, 2011.
51. G.C. Nayak, J.-W. Qiu, and G.F. Sterman, Phys. Rev. **D72**, 114012 (2005).
52. V.N. Gribov and L.N. Lipatov, Sov. J. Nucl. Phys. **15**, 438 (1972);
    L.N. Lipatov, Sov. J. Nucl. Phys. **20**, 94 (1975);
    G. Altarelli and G. Parisi, Nucl. Phys. **B126**, 298 (1977);
    Yu.L. Dokshitzer, Sov. Phys. JETP **46**, 641 (1977).
53. G. Curci, W. Furmanski, and R. Petronzio, Nucl. Phys. **B175**, 27 (1980);
    W. Furmanski and R. Petronzio, Phys. Lett. **B97**, 437 (1980).
54. A. Vogt, S. Moch, and J.A.M. Vermaseren, Nucl. Phys. **B691**, 129 (2004);
    S. Moch, J.A.M. Vermaseren, and A. Vogt, Nucl. Phys. **B688**, 101 (2004).
55. S. Moch *et al.*, arXiv:1707.08315 [hep-ph].
56. S. Moch, J.A.M. Vermaseren, and A. Vogt, Nucl. Phys. **B889**, 351 (2014).
57. D. de Florian, G.F.R. Sborlini, and G. Rodrigo, Eur. Phys. J. **C76**, 282 (2016);
    D. de Florian, G.F.R. Sborlini, and G. Rodrigo, JHEP **1610**, 056 (2016).
58. R.S. Thorne, Phys. Rev. **D73**, 054019 (2006).

59. S. Forte *et al.*, Nucl. Phys. **B834**, 116 (2010).
60. M. Guzzi *et al.*, Phys. Rev. **D86**, 053005 (2012).
61. J.C. Collins, D.E. Soper, and G. Sterman, Nucl. Phys. **B261**, 104 (1985).
62. R. Hamberg, W.L. van Neerven, and T. Matsuura, Nucl. Phys. **B359**, 343 (1991); Erratum *ibid.*, B **644** 403, (2002).
63. R.V. Harlander and W.B. Kilgore, Phys. Rev. Lett. **88**, 201801 (2002).
64. O. Brein, A. Djouadi, and R. Harlander, Phys. Lett. **B579**, 149 (2004).
65. P. Bolzoni *et al.*, Phys. Rev. Lett. **105**, 011801 (2010).
66. D. de Florian and J. Mazzitelli, Phys. Rev. Lett. **111**, 201801 (2013).
67. M. Czakon, P. Fiedler, and A. Mitov, Phys. Rev. Lett. **110**, 252004 (2013).
68. T. Gehrmann *et al.*, Phys. Rev. Lett. **113**, 21 (2014).
69. F. Cascioli *et al.*, Phys. Lett. **B735**, 311 (2014).
70. C. Anastasiou *et al.*, Phys. Rev. Lett. **114**, 21 (2015); C. Anastasiou *et al.*, JHEP **1605**, 058 (2016).
71. F.A. Dreyer and A. Karlberg, Phys. Rev. Lett. **117**, 072001 (2016).
72. D. de Florian *et al.* [LHC Higgs Cross Section Working Group], `arXiv:1610.07922 [hep-ph]`.
73. M. Greco and A. Vicini, Nucl. Phys. **B415**, 386 (1994).
74. L.N. Lipatov, Sov. J. Nucl. Phys. **23**, 338 (1976) [Yad. Fiz. **23**, 642 (1976)].
75. E.A. Kuraev, L.N. Lipatov, and V.S. Fadin, Sov. Phys. JETP **45**, 199 (1977) [Zh. Eksp. Teor. Fiz. **72**, 377 (1977)].
76. I.I. Balitsky and L.N. Lipatov, Sov. J. Nucl. Phys. **28**, 822 (1978) [Yad. Fiz. **28**, 1597 (1978)].
77. V.S. Fadin and L.N. Lipatov, Phys. Lett. **B429**, 127 (1998).
78. M. Ciafaloni and G. Camici, Phys. Lett. **B430**, 329 (1998).
79. G. Altarelli, R.D. Ball, and S. Forte, Nucl. Phys. **B799**, 199 (2008).
80. M. Ciafaloni *et al.*, JHEP **0708**, 046 (2007).
81. C.D. White and R.S. Thorne, Phys. Rev. **D75**, 034005 (2007).
82. E. Iancu *et al.*, Phys. Lett. **B744**, 293 (2015).
83. N. Gromov, F. Levkovich-Maslyuk, and G. Sizov, `arXiv:1507.04010 [hep-th]`; V. N. Velizhanin, `arXiv:1508.02857 [hep-th]`; S. Caron-Huot and M. Herranen, `arXiv:1604.07417 [hep-ph]`.
84. I. Balitsky, Nucl. Phys. **B463**, 99 (1996).
85. Y.V. Kovchegov, Phys. Rev. **D60**, 034008 (1999).
86. A. Hebecker, Phys. Reports **331**, 1 (2000).
87. A.V. Belitsky and A.V. Radyushkin, Phys. Reports **418**, 1 (2005).
88. E. Boos *et al.*, [CompHEP Collab.], Nucl. Instrum. Methods **A534**, 250 (2004) `http://comphep.sinp.msu.ru/`.
89. J. Alwall *et al.*, JHEP **1407**, 079 (2014), `https://launchpad.net/mg5amcnlo`.
90. M.L. Mangano *et al.*, JHEP **0307**, 001 (2003), `http://cern.ch/mlm/alpgen/`.
91. T. Gleisberg and S. Höche, JHEP **0812**, 039 (2008), `https://sherpa.hepforge.org/trac/wiki`.
92. A. Cafarella, C.G. Papadopoulos, and M. Worek, Comp. Phys. Comm. **180**, 1941 (2009), `http://cern.ch/helac-phegas/`.

93. F.A. Berends and W.T. Giele, Nucl. Phys. **B306**, 759 (1988).
94. L.J. Dixon, arXiv:hep-ph/9601359.
95. Z. Bern, L.J. Dixon, and D.A. Kosower, Ann. Phys. **322**, 1587 (2007).
96. S. Badger *et al.*, Phys. Rev. **D87**, 3 (2013).
97. S. Catani and M.H. Seymour, Nucl. Phys. **B485**, 291 (1997) [Erratum-ibid. B **510**,503 (1998)].
98. S. Frixione, Z. Kunszt, and A. Signer, Nucl. Phys. **B467**, 399 (1996).
99. D.A. Kosower, Phys. Rev. **D57**, 5410 (1998);
J.M. Campbell, M.A. Cullen, and E.W.N. Glover, Eur. Phys. J. **C9**, 245 (1999);
D.A. Kosower, Phys. Rev. **D71**, 045016 (2005).
100. Z. Nagy, Phys. Rev. **D68**, 094002 (2003), http://www.desy.de/~znagy/Site/NLOJet++.html.
101. J.M. Campbell and R.K. Ellis, Phys. Rev. **D62**, 114012 (2000).
102. K. Arnold *et al.*, arXiv:1107.4038 [hep-ph];
http://www-itp.particle.uni-karlsruhe.de/~vbfnloweb/.
103. T. Binoth *et al.*, Eur. Phys. J. **C16**, 311 (2000), http://lapth.in2p3.fr/PHOX_FAMILY/.
104. G. Bevilacqua *et al.*, Comp. Phys. Comm. **184**, 986 (2013), http://cern.ch/helac-phegas/.
105. G. Cullen *et al.*, Eur. Phys. J. **C74**, 8 (2014), http://gosam.hepforge.org/.
106. S. Badger *et al.*, Comp. Phys. Comm. **184**, 1981 (2013), https://bitbucket.org/njet/njet/wiki/Home.
107. F. Cascioli, P. Maierhofer, and S. Pozzorini, Phys. Rev. Lett. **108**, 111601 (2012), https://openloops.hepforge.org/.
108. S. Actis *et al.*, Comp. Phys. Comm. **214**, 140 (2017).
109. T. Gleisberg *et al.*, JHEP **0902**, 007 (2009), http://projects.hepforge.org/sherpa/.
110. Z. Bern *et al.*, PoS LL **2012**,018 (2012).
111. Z. Bern *et al.*, Comp. Phys. Comm. **185**, 1443 (2014).
112. T. Kluge, K. Rabbertz, and M. Wobisch, arXiv:hep-ph/0609285, http://fastnlo.hepforge.org/.
113. T. Carli *et al.*, Eur. Phys. J. **C66**, 503 (2010), https://applgrid.hepforge.org/.
114. L. Del Debbio, N.P. Hartland, and S. Schumann, Comp. Phys. Comm. **185**, 2115 (2014), http://mcgrid.hepforge.org/.
115. V. Bertone *et al.*, JHEP **1408**, 166 (2014), https://amcfast.hepforge.org/.
116. G. Cullen, N. Greiner, and G. Heinrich, Eur. Phys. J. **C73**, 4 (2013).
117. S. Kallweit *et al.*, JHEP **1504**, 012 (2015).
118. A. Denner *et al.*, JHEP **1504**, 018 (2015).
119. S. Frixione *et al.*, JHEP **1506**, 184 (2015).
120. R.K. Ellis *et al.*, Phys. Reports **518**, 141 (2012).
121. S. Becker *et al.*, Phys. Rev. Lett. **108**, 032005 (2012).
122. Z. Bern *et al.*, Phys. Rev. **D88**, 014025 (2013).
123. S. Badger *et al.*, Phys. Rev. **D89**, 3 (2014).
124. Z. Bern *et al.*, Nucl. Phys. **B425**, 217 (1994).

125. J.M. Campbell and E.W.N. Glover, Nucl. Phys. **B527**, 264 (1998).
126. S. Catani and M. Grazzini, Phys. Lett. **B446**, 143 (1999).
127. T. Binoth and G. Heinrich, Nucl. Phys. **B585**, 741 (2000).
128. C. Anastasiou, K. Melnikov, and F. Petriello, Phys. Rev. **D69**, 076010 (2004).
129. A. Gehrmann-De Ridder, T. Gehrmann, and E.W.N. Glover, JHEP **0509**, 056 (2005).
130. G. Somogyi, Z. Trocsanyi, and V. Del Duca, JHEP **0701**, 070 (2007).
131. M. Czakon, Phys. Lett. **B693**, 259 (2010).
132. S. Catani and M. Grazzini, Phys. Rev. Lett. **98**, 222002 (2007), `http://theory.fi.infn.it/grazzini/codes.html`.
133. R. Boughezal *et al.*, Phys. Rev. Lett. **115**, 6 (2015).
134. J. Gaunt *et al.*, `arXiv:1505.04794 [hep-ph]`.
135. M. Cacciari *et al.*, `arXiv:1506.02660 [hep-ph]`.
136. A. Gehrmann-De Ridder *et al.*, Phys. Rev. Lett. **99**, 132002 (2007); JHEP **0712**, 094 (2007); Phys. Rev. Lett. **100**, 172001 (2008).
137. A. Gehrmann-De Ridder *et al.*, Comp. Phys. Comm. **185**, 3331 (2014), `https://eerad3.hepforge.org/`.
138. S. Weinzierl, Phys. Rev. Lett. **101**, 162001 (2008); JHEP **0906**, 041 (2009).
139. J. Currie, T. Gehrmann, and J. Niehues, Phys. Rev. Lett. **117**, 042001 (2016).
140. K. Melnikov and F. Petriello, Phys. Rev. **D74**, 114017 (2006), `http://gate.hep.anl.gov/fpetriello/FEWZ.html`.
141. S. Catani *et al.*, Phys. Rev. Lett. **103**, 082001 (2009), `http://theory.fi.infn.it/grazzini/dy.html`.
142. C. Anastasiou, K. Melnikov, and F. Petriello, Nucl. Phys. **B724**, 197 (2005), `http://www.phys.ethz.ch/~pheno/fehipro/`.
143. S. Borowka *et al.*, Phys. Rev. Lett. **117**, 012001 (2016) Erratum:[Phys. Rev. Lett. **117**, 079901 (2016).
144. G. Ferrera, M. Grazzini, and F. Tramontano, Phys. Rev. Lett. **107**, 152003 (2011).
145. G. Ferrera, M. Grazzini, and F. Tramontano, Phys. Lett. **B740**, 51 (2015).
146. M. Grazzini *et al.*, JHEP **1705**, 139 (2017).
147. S. Catani *et al.*, Phys. Rev. Lett. **108**, 072001 (2012).
148. J.M. Campbell *et al.*, JHEP **1607**, 148 (2016).
149. M. Grazzini *et al.*, Phys. Lett. **B731**, 204 (2014).
150. M. Grazzini, S. Kallweit, and D. Rathlev, JHEP **1507**, 085 (2015).
151. R. Boughezal *et al.*, Eur. Phys. J. **C77**, 7 (2017).
152. R. Boughezal *et al.*, `arXiv:1504.07922 [hep-ph]`.
153. R. Boughezal *et al.*, Phys. Lett. **B748**, 5 (2015).
154. F. Caola, K. Melnikov and M. Schulze, Phys. Rev. **D92**, 074032 (2015).
155. X. Chen *et al.*, JHEP **1610**, 066 (2016).
156. A. Gehrmann-De Ridder *et al.*, Phys. Rev. Lett. **117**, 022001 (2016).
157. R. Boughezal *et al.*, Phys. Rev. Lett. **116**, 152001 (2016).
158. J.M. Campbell, R.K. Ellis, and C. Williams, Phys. Rev. Lett. **118**, 222001 (2017).

159. M. Brucherseifer, F. Caola, and K. Melnikov, Phys. Lett. **B736**, 58 (2014).
160. E.L. Berger *et al.*, Phys. Rev. **D94**, 071501 (2016).
161. M. Czakon, P. Fiedler, and A. Mitov, Phys. Rev. Lett. **115**, 5 (2015).
162. J. Currie, E.W.N. Glover, and J. Pires, Phys. Rev. Lett. **118**, 072002 (2017).
163. Y.L. Dokshitzer, D.Diakonov, and S.I. Troian, Phys. Reports **58**, 269 (1980).
164. G. Parisi and R. Petronzio, Nucl. Phys. **B154**, 427 (1979).
165. G. Curci, M. Greco, and Y. Srivastava, Nucl. Phys. **B159**, 451 (1979).
166. A. Bassetto, M. Ciafaloni, and G. Marchesini, Nucl. Phys. **B163**, 477 (1980).
167. J.C. Collins and D.E. Soper, Nucl. Phys. **B193**, 381 (1981) [Erratum-*ibid.* **B213**, 545 (1983)].
168. J.C. Collins and D.E. Soper, Nucl. Phys. **B197**, 446 (1982).
169. J. Kodaira and L. Trentadue, Phys. Lett. **B112**, 66 (1982).
170. J. Kodaira and L. Trentadue, Phys. Lett. **B123**, 335 (1983).
171. J.C. Collins, D.E. Soper, and G. Sterman, Nucl. Phys. **B250**, 199 (1985).
172. S. Catani *et al.*, Nucl. Phys. **B407**, 3 (1993).
173. C. W. Bauer *et al.*, Phys. Rev. **D63**, 114020 (2001).
174. C.W. Bauer, D. Pirjol, and I.W. Stewart, Phys. Rev. **D65**, 054022 (2002).
175. T. Becher, A. Broggio, and A. Ferroglia, Lect. Notes Phys. **896** (2015) pp.1 `arXiv:1410.1892 [hep-ph]`.
176. S. Catani *et al.*, Phys. Lett. **B269**, 432 (1991).
177. N. Brown and W.J. Stirling, Phys. Lett. **B252**, 657 (1990).
178. W. Bartel *et al.*, [JADE Collab.], Z. Phys. **C33**, 23 (1986).
179. N. Kidonakis, G. Oderda, and G. Sterman, Nucl. Phys. **B531**, 365 (1998).
180. R. Bonciani *et al.*, Phys. Lett. **B575**, 268 (2003).
181. A. Banfi, G.P. Salam, and G. Zanderighi, JHEP **0503**, 073 (2005).
182. D. de Florian and M. Grazzini, Phys. Rev. Lett. **85**, 4678 (2000).
183. G. Bozzi *et al.*, Nucl. Phys. **B737**, 73 (2006), `http://theory.fi.infn.it/grazzini/codes.html`.
184. G. Bozzi *et al.*, Phys. Lett. **B696**, 207 (2011).
185. T. Becher and M. Neubert, Eur. Phys. J. **C71**, 1665 (2011).
186. T. Becher, M. Neubert, and D. Wilhelm, `http://cute.hepforge.org/`.
187. D. de Florian *et al.*, JHEP **1206**, 132 (2012), `http://theory.fi.infn.it/grazzini/codes.html`.
188. C. Balazs and C.P. Yuan, Phys. Rev. **D56**, 5558 (1997).
189. S. Catani *et al.*, `arXiv:1507.06937 [hep-ph]`.
190. A. Banfi *et al.*, Phys. Lett. **B715**, 152 (2012).
191. M. Grazzini *et al.*, `arXiv:1507.02565 [hep-ph]`.
192. D. de Florian and M. Grazzini, Nucl. Phys. **B704**, 387 (2005).
193. T. Becher and G. Bell, JHEP **1211**, 126 (2012).
194. A. Banfi *et al.*, Phys. Rev. Lett. **109**, 202001 (2012);
T. Becher, M. Neubert, and L. Rothen, JHEP **1310**, 125 (2013);
I.W. Stewart *et al.*, Phys. Rev. **D89**, 5 (2014).
195. I.W. Stewart, F.J. Tackmann, and W.J. Waalewijn, Phys. Rev. Lett. **106**, 032001 (2011).

196. Y.-T. Chien *et al.*, Phys. Rev. **D87**, 014010 (2013);
T.T. Jouttenus *et al.*, Phys. Rev. **D88**, 054031 (2013).
197. M. Dasgupta *et al.*, JHEP **1210**, 126 (2012).
198. V. Ahrens *et al.*, JHEP **1009**, 097 (2010).
199. M. Aliev *et al.*, Comp. Phys. Comm. **182**, 1034 (2011).
200. N. Kidonakis, Phys. Rev. **D82**, 114030 (2010).
201. T. Becher, C. Lorentzen, M. D. Schwartz, Phys. Rev. Lett. **108**, 012001 (2012).
202. T. Becher *et al.*, Eur. Phys. J. **C75**, 4 (2015).
203. E. Gerwick *et al.*, JHEP **1502**, 106 (2015).
204. A. Banfi *et al.*, JHEP **1505**, 102 (2015).
205. T. Becher and M.D. Schwartz, JHEP **0807**, 034 (2008).
206. A. H. Hoang *et al.*, Phys. Rev. **D91**, 9 (2015).
207. Y.-T. Chien and M.D. Schwartz, JHEP **1008**, 058 (2010).
208. P.F. Monni, T. Gehrmann, and G. Luisoni, JHEP **1108**, 010 (2011).
209. W. Bizon *et al.*, `arXiv:1705.09127 [hep-ph]`.
210. S. Catani *et al.*, Nucl. Phys. **B888**, 75 (2014).
211. S. Fleming *et al.*, Phys. Rev. **D77**, 074010 (2008).
212. A.H. Hoang, P. Pietrulewicz, and D. Samitz, Phys. Rev. **D93**, 034034 (2016).
213. I. Feige *et al.*, Phys. Rev. Lett. **109**, 092001 (2012).
214. M. Dasgupta *et al.*, JHEP **1309**, 029 (2013).
215. A.J. Larkoski *et al.*, JHEP **1405**, 146 (2014).
216. M. Dasgupta, A. Powling, and A. Siodmok, `arXiv:1503.01088 [hep-ph]`.
217. A.J. Larkoski, I. Moult, and D. Neill, `arXiv:1507.03018 [hep-ph]`.
218. Yu.L. Dokshitzer *et al.*, *"Basics of perturbative QCD,"* Gif-sur-Yvette, France: Éditions frontières (1991), see also `http://www.lpthe.jussieu.fr/~yuri/BPQCD/cover.html`.
219. T. Sjöstrand *et al.*, Comp. Phys. Comm. **135**, 238 (2001).
220. T. Sjöstrand, S. Mrenna, and P. Skands, JHEP **0605**, 026 (2006), `http://projects.hepforge.org/pythia6/`.
221. T. Sjöstrand *et al.*, Comp. Phys. Comm. **191**, 159 (2015), `http://home.thep.lu.se/~torbjorn/Pythia.html`.
222. B.R. Webber, Nucl. Phys. **B238**, 492 (1984).
223. G. Corcella *et al.*, JHEP **0101**, 010 (2001), `http://www.hep.phy.cam.ac.uk/theory/webber/Herwig/`.
224. M. Bahr *et al.*, Eur. Phys. J. **C58**, 639 (2008), `http://projects.hepforge.org/herwig/`.
225. L. Lönnblad, Comp. Phys. Comm. **71**, 15, (1992).
226. A. Buckley *et al.*, Phys. Rept. **504**, 145-233 (2011).
227. B. Andersson *et al.*, Phys. Reports **97**, 31 (1983).
228. T. Sjöstrand, Nucl. Phys. **B248**, 469 (1984).
229. T. Sjöstrand and M. van Zijl, Phys. Rev. **D36**, 2019 (1987).
230. S. Catani *et al.*, JHEP **0111**, 063 (2001).
231. J. Alwall *et al.*, Eur. Phys. J. **C53**, 473 (2008).
232. S. Frixione and B.R. Webber, JHEP **0206**, 029 (2002).

233. P. Nason, JHEP **0411**, 040 (2004).
234. S. Alioli *et al.*, JHEP **1006**, 043 (2010), `http://powhegbox.mib.infn.it/`.
235. S. Höche *et al.*, JHEP **1209**, 049 (2012).
236. S. Höche *et al.*, JHEP **1304**, 027 (2013);
R. Frederix and S. Frixione, JHEP **1212**, 061 (2012);
S. Plätzer, JHEP **1308**, 114 (2013);
L. Lönnblad and S. Prestel, JHEP **1303**, 166 (2013);
K. Hamilton *et al.*, JHEP **1305**, 082 (2013).
237. K. Hamilton *et al.*, JHEP **1310**, 222 (2013);
A. Karlberg, E. Re, and G. Zanderighi, JHEP **1409**, 134 (2014);
S. Höche, Y. Li and S. Prestel, Phys. Rev. **D91**, 074015 (2015);
S. Höche, Y. Li and S. Prestel, Phys. Rev. **D90**, 054011 (2014);
S. Alioli *et al.*, Phys. Rev. **D92**, 094020 (2015).
238. P.M. Stevenson, Phys. Lett. **B100**, 61 (1981).
239. P.M. Stevenson, Phys. Rev. **D23**, 2916 (1981).
240. G. Grunberg, Phys. Rev. **D29**, 2315 (1984).
241. S.J. Brodsky, G.P. Lepage, and P.B. Mackenzie, Phys. Rev. **D28**, 228 (1983).
242. M. Cacciari and N. Houdeau, JHEP **1109**, 039 (2011).
243. A. David and G. Passarino, Phys. Lett. **B726**, 266 (2013).
244. E. Bagnaschi *et al.*, JHEP **1502**, 133 (2015).
245. M. Cacciari *et al.*, JHEP **0404**, 068 (2004).
246. M. Dasgupta and G.P. Salam, J. Phys. **G30**, R143 (2004).
247. S. Moretti, L. Lönnblad, and T. Sjöstrand, JHEP **9808**, 001 (1998).
248. G.P. Salam, Eur. Phys. J. **C67**, 637 (2010).
249. S.D. Ellis *et al.*, Prog. in Part. Nucl. Phys. **60**, 484 (2008).
250. M. Cacciari, Int. J. Mod. Phys. **A30**, 1546001 (2015).
251. G.P. Salam and G. Soyez, JHEP **0705**, 086 (2007).
252. S. Catani *et al.*, Nucl. Phys. **B406**, 187 (1993).
253. S.D. Ellis and D.E. Soper, Phys. Rev. **D48**, 3160 (1993).
254. Y.L. Dokshitzer *et al.*, JHEP **9708**, 001 (1997).
255. M. Wobisch and T. Wengler, `arXiv:hep-ph/9907280`.
256. M. Cacciari, G.P. Salam, and G. Soyez, JHEP **0804**, 063 (2008).
257. S. Bethke *et al.*, Nucl. Phys. **B370**, 310 (1992), Nucl. Phys. **B523**, 681 (1998).
258. M. Cacciari and G.P. Salam, Phys. Lett. **B641**, 57 (2006);
M. Cacciari, G.P. Salam, and G. Soyez, Eur. Phys. J. **C72**, 1896 (2012) `http://fastjet.fr/`.
259. S. Brandt *et al.*, Phys. Lett. **12**, 57 (1964).
260. E. Farhi, Phys. Rev. Lett. **39**, 1587 (1977).
261. O. Biebel, Phys. Reports **340**, 165 (2001).
262. S. Kluth, Rept. on Prog. in Phys. **69**, 1771 (2006).
263. C.L. Basham *et al.*, Phys. Rev. Lett. **41**, 1585 (1978).
264. A. Ali, E. Pietarinen, and W. J. Stirling, Phys. Lett. **B141**, 447 (1984).
265. I. W. Stewart, F. J. Tackmann, and W. J. Waalewijn, Phys. Rev. Lett. **105**, 092002 (2010).

266. A. Banfi, G.P. Salam, and G. Zanderighi, JHEP **0408**, 062 (2004).
267. A. Banfi, G.P. Salam, and G. Zanderighi, JHEP **1006**, 038 (2010).
268. T. Aaltonen *et al.*, [CDF Collab.], Phys. Rev. **D83**, 112007 (2011).
269. G. Aad *et al.*, [ATLAS Collab.], Eur. Phys. J. **C72**, 2211 (2012).
270. G. Aad *et al.*, [ATLAS Collab.], Phys. Rev. **D88**, 032004 (2013).
271. G. Aad *et al.*, [ATLAS Collab.], Phys. Lett. **B750**, 427 (2015).
272. G. Aad *et al.*, [ATLAS Collab.], Eur. Phys. J. **C76**, 375 (2016).
273. M. Aaboud *et al.*, [ATLAS Collab.], `arXiv:1707.02562 [hep-ex]`.
274. V. Khachatryan *et al.*, [CMS Collab.], Phys. Lett. **B699**, 48 (2011).
275. S. Chatrchyan *et al.*, [CMS Collab.], Phys. Lett. **B722**, 238 (2013).
276. V. Khachatryan *et al.*, [CMS Collab.], JHEP **1410**, 87 (2014).
277. S. Chatrchyan *et al.*, [CMS Collab.], Phys. Lett. **B730**, 243 (2014).
278. G. Aad *et al.*, [ATLAS Collab.], Phys. Rev. **D83**, 052003 (2011).
279. S. Chatrchyan *et al.*, [CMS Collab.], JHEP **1206**, 160 (2012).
280. B. B. Abelev *et al.*, [ALICE Collab.], Phys. Rev. **D91**, 112012 (2015).
281. G. Aad *et al.*, [ATLAS Collab.], Eur. Phys. J. **C73**, 2676 (2013).
282. C. Glasman [H1 Collab. and ZEUS Collab.], Nucl. Phys. (Proc. Supp.) **191**, 121 (2009).
283. T. Carli, K. Rabbertz, and S. Schumann, `arXiv:1506.03239 [hep-ex]`.
284. A. Abdesselam *et al.*, Eur. Phys. J. **C71**, 1661 (2011).
285. A. Altheimer *et al.*, J. Phys. **G39**, 063001 (2012).
286. A. Altheimer *et al.*, Eur. Phys. J. **C74**, 2792 (2014).
287. S. Schaetzel, Eur. Phys. J. **C75**, 9 (2015).
288. A. J. Larkoski, I. Moult, and B. Nachman, `arXiv:1709.04464 [hep-ph]`.
289. D. Adams *et al.*, Eur. Phys. J. **C75**, 409 (2015).
290. T. Schörner-Sadenius, Eur. Phys. J. **C72**, 2060 (2012).
291. J.M. Campbell, J.W. Huston, and W.J. Stirling, Rept. on Prog. in Phys. **70**, 89 (2007).
292. M.L. Mangano, Phys. Usp. **53**, 109 (2010).
293. J.M. Butterworth, G. Dissertori, and G.P. Salam, Ann. Rev. Nucl. and Part. Sci. **62**, 387 (2012).
294. T. Carli, T. Gehrmann, and S. Höche, Eur. Phys. J. **C67**, 73 (2010).
295. F.D. Aaron *et al.*, [H1 Collab.], Eur. Phys. J. **C65**, 363 (2010).
296. F.D. Aaron *et al.*, [H1 Collab.], Eur. Phys. J. **C54**, 389 (2008).
297. S. Chekanov *et al.*, [ZEUS Collab.], Eur. Phys. J. **C52**, 515 (2007).
298. S. Chekanov *et al.*, [ZEUS Collab.], Phys. Rev. **D78**, 032004 (2008).
299. H. Abramowicz *et al.*, [ZEUS Collab.], Eur. Phys. J. **C70**, 965 (2010).
300. H. Abramowicz *et al.*, [ZEUS Collab.], Phys. Lett. **B691**, 127 (2010).
301. S. Chekanov *et al.*, [ZEUS Collab.], Phys. Rev. **D85**, 052008 (2012).
302. F.D. Aaron *et al.*, [H1 Collab.], Eur. Phys. J. **C67**, 1 (2010).
303. V. Andreev *et al.*, [H1 Collab.], Eur. Phys. J. **C75**, 2 (2015).
304. S. Chekanov *et al.*, [ZEUS Collab.], Nucl. Phys. **B792**, 1 (2008).
305. S. Chekanov *et al.*, [ZEUS Collab.], Phys. Rev. **D76**, 072011 (2007).
306. A. Aktas *et al.*, [H1 Collab.], Phys. Lett. **B639**, 21 (2006).

307. H. Abramowicz *et al.*, [ZEUS Collab.], Eur. Phys. J. **C71**, 1659 (2011).
308. H. Abramowicz *et al.*, [ZEUS Collab.], Nucl. Phys. **B864**, 1 (2012).
309. `http://atlas.web.cern.ch/Atlas/GROUPS/PHYSICS/CombinedSummaryPlots/SM`.
310. `http://twiki.cern.ch/twiki/bin/view/CMSPublic/PhysicsResultsCombined`.
311. A. Abulencia *et al.*, [CDF - Run II Collab.], Phys. Rev. **D75**, 092006 (2007) [Erratum-ibid. 119901].
312. V.M. Abazov *et al.*, [D0 Collab.], Phys. Rev. Lett. **101**, 062001 (2008).
313. V.M. Abazov *et al.*, [D0 Collab.], Phys. Rev. **D85**, 052006 (2012).
314. B. Abelev *et al.*, [ALICE Collab.], Phys. Lett. **B722**, 262 (2013).
315. G. Aad *et al.*, [ATLAS Collab.], Eur. Phys. J. **C73**, 2509 (2013).
316. G. Aad *et al.*, [ATLAS Collab.], JHEP **1502**, 153 (2015), erratum JHEP **1509**, 141 (2015).
317. M. Aaboud *et al.*, [ATLAS Collab.], JHEP **1709**, 020 (2017).
318. V. Khachatryan *et al.*, [CMS Collab.], Eur. Phys. J. **C76**, 265 (2016).
319. S. Chatrchyan *et al.*, [CMS Collab.], Phys. Rev. **D87**, 112002 (2013).
320. V. Khachatryan *et al.*, [CMS Collab.], JHEP **1703**, 156 (2017).
321. V. Khachatryan *et al.*, [CMS Collab.], Eur. Phys. J. **C76**, 451 (2016).
322. M. Wobisch *et al.*, [fastNLO Collab.], `arXiv:1109.1310 [hep-ph]`.
323. P. Francavilla, Int. J. Mod. Phys. **A30**, 1546003 (2015).
324. A. Schwartzman, Int. J. Mod. Phys. **A30**, 1546002 (2015).
325. J. Rojo, Int. J. Mod. Phys. **A30**, 1546005 (2015).
326. G. Aad *et al.*, [ATLAS Collab.], JHEP **1405**, 059 (2014).
327. A. M. Sirunyan *et al.*, [CMS Collab.], `arXiv:1705.02628 [hep-ex]`.
328. T. Aaltonen *et al.*, [CDF Collab.], Phys. Rev. **D79**, 112002 (2009).
329. V.M. Abazov *et al.*, [D0 Collab.], Phys. Rev. Lett. **103**, 191803 (2009).
330. S. Chatrchyan *et al.*, [CMS Collab.], JHEP **1205**, 055 (2012).
331. V. Khachatryan *et al.*, [CMS Collab.], Phys. Lett. **B746**, 79 (2015).
332. A.M. Sirunyan *et al.*, [CMS Collab.], JHEP **1707**, 013 (2017).
333. G. Aad *et al.*, [ATLAS Collab.], JHEP **1301**, 029 (2013).
334. M. Aaboud *et al.*, [ATLAS Collab.], `arXiv:1703.09127 [hep-ex]`.
335. V.M. Abazov *et al.*, [D0 Collab.], Phys. Rev. Lett. **94**, 221801 (2005).
336. V.M. Abazov *et al.*, [D0 Collab.], Phys. Lett. **B721**, 212 (2013).
337. G. Aad *et al.*, [ATLAS Collab.], Phys. Rev. Lett. **106**, 172002 (2011).
338. V. Khachatryan *et al.*, [CMS Collab.], Phys. Rev. Lett. **106**, 122003 (2011).
339. V. Khachatryan *et al.*, [CMS Collab.], Eur. Phys. J. **C76**, 536 (2016).
340. M. Campanelli, Int. J. Mod. Phys. **A30**, 1546006 (2015).
341. P. Kokkas, Int. J. Mod. Phys. **A30**, 1546004 (2015).
342. M. Aaboud *et al.*, [ATLAS Collab.], Eur. Phys. J. **C77**, 367 (2017).
343. G. Aad *et al. et al.*, [ATLAS Collab.], Phys. Lett. **B759**, 601 (2016).
344. S. Chatrchyan *et al.*, [CMS Collab.], JHEP **1110**, 132 (2011).
345. S. Chatrchyan *et al.*, [CMS Collab.], Phys. Rev. Lett. **112**, 191802 (2014).
346. R. Aaij *et al.*, [LHCb Collab.], JHEP **1206**, 058 (2012).
347. R. Aaij *et al.*, [LHCb Collab.], JHEP **1601**, 155 (2016).

348. R. Aaij *et al.*, [LHCb Collab.], JHEP **1609**, 136 (2016).
349. S. Chatrchyan *et al.*, [CMS Collab.], JHEP **1110**, 007 (2011).
350. V. Khachatryan *et al.*, [CMS Collab.], Eur. Phys. J. **C75**, 147 (2015).
351. G. Aad *et al.*, [ATLAS Collab.], Phys. Lett. **B725**, 223 (2013).
352. G. Aad *et al.*, [ATLAS Collab.], JHEP **1406**, 112 (2014).
353. G. Aad *et al.*, [ATLAS Collab.], JHEP **1608**, 009 (2016).
354. S. Chatrchyan *et al.*, [CMS Collab.], Phys. Rev. **D90**, 3 (2014).
355. V. Khachatryan *et al.*, [CMS Collab.], Eur. Phys. J. **C76**, 469 (2016).
356. G. Aad *et al.*, [ATLAS Collab.], Eur. Phys. J. **C76**, 291 (2016).
357. V. Khachatryan *et al.*, [CMS Collab.], JHEP **1702**, 096 (2017).
358. U. Blumenschein, Int. J. Mod. Phys. **A30**, 1546007 (2015).
359. G. Aad *et al.*, [ATLAS Collab.], JHEP **1307**, 032 (2013).
360. J. H. Kühn *et al.*, JHEP **0603**, 059 (2006).
361. V. Khachatryan *et al.*, [CMS Collab.], JHEP **1510**, 128 (2015), erratum JHEP **1604**, 010 (2016).
362. M. Voutilainen, Int. J. Mod. Phys. **A30**, 1546008 (2015).
363. G. Aad *et al.*, [ATLAS Collab.], JHEP **1609**, 029 (2016).
364. M. Aaboud *et al.*, [ATLAS Collab.], Phys. Lett. **B773**, 354 (2017).
365. V. Khachatryan *et al.*, [CMS Collab.], Eur. Phys. J. **C76**, 401 (2016).
366. G. Aad *et al.*, [ATLAS Collab.], JHEP **1301**, 086 (2013).
367. M. Aaboud *et al.*, [ATLAS Collab.], Phys. Rev. **D95**, 112005 (2017).
368. S. Chatrchyan *et al.*, [CMS Collab.], Eur. Phys. J. **C74**, 3129 (2014).
369. K. Kröninger, A. B. Meyer, and P. Uwer, `arXiv:1506.02800 [hep-ex]`.
370. S. Chatrchyan *et al.*, [CMS Collab.], Phys. Lett. **B728**, 496 (2014), Phys. Lett. **B728**, 526 (2014).
371. T. Klijnsma, S. Bethke, G. Dissertori, and G. P. Salam, `arXiv:1708.07495 [hep-ph]`.
372. G. Aad *et al.*, [ATLAS Collab.], Eur. Phys. J. **C74**, 10 (2014).
373. A.M. Sirunyan *et al.*, [CMS Collab.], JHEP **1709**, 051 (2017).
374. G. Aad *et al.*, [ATLAS Collab.], Phys. Rev. Lett. **115**, 091801 (2015).
375. G. Aad *et al.*, [ATLAS Collab.], JHEP **1608**, 104 (2016).
376. M. Aaboud *et al.*, [ATLAS Collab.], `arXiv:1708.02810 [hep-ex]`.
377. S. Chatrchyan *et al.*, [CMS Collab.], Phys. Rev. **D89**, 9 (2014).
378. V. Khachatryan *et al.*, [CMS Collab.], Eur. Phys. J. **C76**, 13 (2016).
379. V. Khachatryan *et al.*, [CMS Collab.], JHEP **1604**, 005 (2016).
380. V. Khachatryan *et al.*, [CMS Collab.], JHEP **1703**, 032 (2017).
381. S. Bethke, G. Dissertori and G.P. Salam in [382].
382. C. Patrignani *et al.*, [Particle Data Group Collaboration], Chin. Phys. **C40** (2016) 100001.
383. S. Bethke, Prog. in Part. Nucl. Phys. **58**, 351 (2007).
384. S. Bethke, Eur. Phys. J. **C64**, 689 (2009).
385. S. Bethke, J. Phys. **G26**, R27 (2000).
386. M. Schmelling, Phys. Scripta **51**, 676 (1995).
387. M. Beneke and M. Jamin, JHEP **0809**, 044 (2008).

388. K. Maltman and T. Yavin, Phys. Rev. **D78**, 094020 (2008).
389. S. Narison, Phys. Lett. **B673**, 30 (2009).
390. I. Caprini and J. Fischer, Eur. Phys. J. **C64**, 35 (2009).
391. A. Pich, Prog. in Part. Nucl. Phys. **75**, 41 (2014).
392. M. Davier *et al.*, Eur. Phys. J. **C74**, 2803 (2014).
393. D. Boito *et al.*, Phys. Rev. D 91,034003(2015).
394. G. Altarelli, PoS Corfu **2012** (2013) 002.
395. C. McNeile *et al.*, [HPQCD Collab.], Phys. Rev. **D82**, 034512 (2010).
396. C.T.H. Davies *et al.*, [HPQCD Collab., UKQCD Collab., and MILC Collab.], Phys. Rev. Lett. **92**, 022001 (2004).
397. K. Maltman *et al.*, Phys. Rev. **D78**, 114504 (2008).
398. B. Chakraborty *et al.*, [HPQCD Collab.], Phys. Rev. **D91**, 054508 (2015).
399. S. Aoki *et al.*, [PACS-CS Collab.], JHEP **0910**, 053 (2009).
400. B. Blossier *et al.*, [ETM Collab.], Phys. Rev. Lett. **108**, 262002 (2012), Phys. Rev. **D89**, 014507 (2014).
401. A. Bazavov *et al.*, [BBGPSV], Phys. Rev. **D90**, 074038 (2014).
402. E. Shintani *et al.*, [JLQCD Collab.], Phys. Rev. **D82**, 074505 (2010), erratum Phys. Rev. **D89**, 099903 (2014).
403. S. Aoki *et al.*, Eur. Phys. J. **C74**, 2890 (2014).
404. C. Glasman [H1 Collab. and ZEUS Collab.], J. Phys. Conf. Ser. **110** 022013 (2008).
405. V. Andreev *et al.*, (H1 Collab.), Eur. Phys. J. **C75**, 65 (2015).
406. T. Biekötter, M. Klasen and G. Kramer, Phys. Rev. **D92**, 074037 (2015).
407. J. Blümlein, H. Bottcher, and A. Guffanti, Nucl. Phys. **B774**, 182 (2007).
408. S. Alekhin, J. Blümlein, and S. Moch, Phys. Rev. **D86**, 054009 (2012).
409. P. Jimenez-Delgado and E. Reya, Phys. Rev. **D79**, 074023 (2009).
410. A. D. Martin *et al.*, Eur. Phys. J. **C64**, 653 (2009).
411. L. A. Harland-Lang *et al.*, Eur. Phys. J. **C75**, 435 (2015).
412. R.D. Ball *et al.*, Phys. Lett. **B707**, 66 (2012).
413. R.S. Thorne and G. Watt, JHEP **1108**, 100 (2011).
414. S. Alekhin, J. Blümlein, and S.Moch, Eur. Phys. J. **C71**, 1723 (2011).
415. R.D. Ball *et al.*, Phys. Lett. **B704**, 36 (2011).
416. R.D. Ball *et al.*, Phys. Lett. **B723**, 330 (2013).
417. R.S. Thorne *et al.*, PoS DIS **2013** (2013) 042.
418. N. Brambilla *et al.*, Phys. Rev. **D75**, 074014 (2007).
419. G. Dissertori *et al.*, JHEP **0908**, 036 (2009).
420. G. Abbiendi *et al.*, Eur. Phys. J. **C71**, 1733 (2011).
421. S. Bethke *et al.*, [JADE Collab.], Eur. Phys. J. **C64**, 351 (2009).
422. G. Dissertori *et al.*, Phys. Rev. Lett. **104**, 072002 (2010).
423. J. Schieck *et al.*, Eur. Phys. J. **C73**, 2332 (2013).
424. R.A. Davison and B.R. Webber, Eur. Phys. J. **C59**, 13 (2009).
425. R. Abbate *et al.*, Phys. Rev. **D83**, 074021 (2011).
426. T. Gehrmann *et al.*, Eur. Phys. J. **C73**, 2265 (2013).
427. A.H. Hoang *et al.*, Phys. Rev. **D91**, 094018 (2015).
428. R. Frederix *et al.*, JHEP **1011**, 050 (2010).

429. P. Bolzoni, B.A. Kniehl, and A.V. Kotikov, Nucl. Phys. **B875**, 18 (2013).
430. M. Abazov *et al.*, [D0 Collab.], Phys. Rev. **D80**, 111107 (2009).
431. M. Abazov *et al.*, [D0 Collab.], Phys. Lett. **B718**, 56 (2012).
432. G. Aad *et al.*, [ATLAS Collab.], Phys. Rev. **D86**, 014022 (2012).
433. B. Malaescu and P. Starovoitov, Eur. Phys. J. **C72**, 2041 (2012).
434. S. Chatrchyan *et al.*, [CMS Collab.], Eur. Phys. J. **C73**, 2604 (2013).
435. V. Khachatryan *et al.*, [CMS Collab.], Eur. Phys. J. **C75**, 288 (2015).
436. V. Khachatryan *et al.*, [CMS Collab.], Eur. Phys. J. **C75**, 186 (2015).
437. M. Baak *et al.*, [Gfitter group], Eur. Phys. J. **C74**, 3046 (2014).